



NTNU – Trondheim
Norwegian University of
Science and Technology

Nanostructured surfaces with patterned wettability

Brita Melberg

Nanotechnology

Submission date: June 2012

Supervisor: Pawel Tadeusz Sikorski, IFY

Co-supervisor: Florian Mumm, IFY

Norwegian University of Science and Technology
Department of Physics

Abstract

This project aims at the fabrication of a rough polydimethylsiloxane(PDMS) surface with patterned smooth areas. The idea is that such a surface will allow for water capturing on the smooth areas of the surface. The applications for this kind of surface are many, but especially the prospects of a surface able to trap droplets of cells in suspension by simply dipping the surface into the suspension is intriguing.

From a previous project[1], and another student's master's thesis[2], the use of an etched copper surface seemed promising for the fabrication of a rough mold. This was abandoned after sandpaper turned out to be an even better mold, giving superhydrophobic PDMS($162, 33 \pm 1, 40^\circ$).

The negative photoresist SU-8 5 was used to pattern the sandpaper with small, circular features on the P1000 sandpaper($400\mu m$ and $1mm$ in diameter). The PDMS replica from this mold was a rough surface with smooth wells. This was not able to capture water droplets effectively, partly because air bubbles were trapped in the wells during the immersion in water. To avoid this, another mold was procured by the silanization of the previously made PDMS surface. The PDMS replica of the silanized PDMS had smooth pillars instead of wells, and did not succeed in trapping water droplets either. In fact, the smooth wells seemed to better at capturing the water.

This project has succeeded in producing high enough roughness on PDMS to alter the contact angle with water by $\sim 61^\circ$ to a contact angle exceeding the lower limit for superhydrophobic surfaces by $\sim 12^\circ$. The use of a sandpaper mold has proven to be simple, inexpensive and effective at producing PDMS with high contact angles.

Sammendrag

Målet til denne oppgaven er å lage en ru polydimetylsiloksan(PDMS) overflate med et mønster av glatte områder. Ideen er at en slik overflate vil være i stand til å fange vann til vandrdåper på de glatte områdene. En slik overflate kan brukes til mange formål, men spesielt muligheten for en overflate som er i stand til å fange dråper av cellulær suspensjon ved å dyppe overflaten i en slik væske er spennende.

Fra et tidligere prosjekt[1] og en annen students masteroppgave[2] har bruken av etsede kobberflater virket som en god metode for å lage en ru form for videre replikasjon. Denne metoden ble lagt til side da sandpapir viste seg å være en bedre form, og var i stand til å produsere superhydrofobisk PDMS($162, 33 \pm 1, 40^\circ$).

Det ble laget et mønster av SU-8 5 sylindre($400\mu m$ og $1mm$ i diameter) ved bruk av fotolitografi på P1000 sandpapir. PDMSreplikasjonen av denne formen var en ru overflate med glatte brønner. Overflaten var ikke i stand til å fange dråper skikkelig, delvis på grunn av luftbobler som ble dannet ved dypping i vann. En ny form ble laget for å unngå dette fenomenet, denne besto av en silanisert, ru PDMS overflate med glatte brønner. PDMS replikasjonen av denne hadde glatte sylindere på overflaten i stedet for brønner. Denne kunne ikke fange dråper på de glatte sylindertoppene. PDMS overflaten med glatte brønner var faktisk bedre egnet, da denne kunne fange litt vann i enkelte brønner.

Dette prosjektet har lyktes med å produsere høy nok ruhet på en PDMSoverflate til å endre kontaktvinkelen med vann med $\sim 61^\circ$ ved kun å endre ruheten, og er $\sim 12^\circ$ over den nedre grensen for en superhydrofobisk overflate. Sandpapir har vist seg å være enkelt, billig og effektiv som form i produksjonen av PDMS med høye kontaktvinkler.

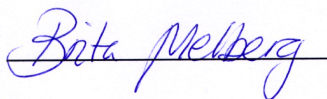
Preface

This thesis is submitted as a part of a Master's degree in Bionanotechnology at Norwegian University of Science and Technology(NTNU). The work was done in the period January–June 2012 at Department of Physics at the Faculty of Natural Sciences and Technology. Associate Professor Pawel Sikorski was the main supervisor and Post-doctoral fellow Florian Mumm was co-supervisor of the project.

The work was the natural extension of the Nanotechnology Specialization Project (TMM4550, 15 ECTS), and some parts of this project is reused in this thesis. Both on that project, and on this, I have received a lot of guidance, training and help that has been invaluable to the thesis. Special thanks to the NTNU NanoLab staff for help and training in the NanoLab, to Gjertrud Maurstad for the help in the biophysics lab, David Barriet for his assistance and training in the silanization process and to Wilhelm Robert Glomm for arranging contact angle measurement training and help. To Kai Beckwith, thanks for suggestions and encouragement. To Linn, thank you for lovely coffee breaks!

However, the absolutely greatest help on this thesis was given by Associate Professor Pawel Sikorski. Thanks for guidance, ideas, suggestions, pushing and discussions that set me on the right course. Thanks to Florian, without the help I received in the start of this project, I would not have as good an understanding or have received as good results. You have been sorely missed.

I hereby declare that this thesis has been written independently and in accordance with the exam regulations for "sivilingeniøreksamen" at the Norwegian University of Science and Technology (NTNU).



Brita Melberg
Trondheim, June 13, 2012

Contents

Abstract	i
Sammendrag	iii
Preface	v
Contents	vii
List of Figures	xi
1 Introduction	3
2 Theory	9
2.1 Contact Angle and Hydrophobicity	10
2.1.1 Contact Angle Hysteresis	12
2.2 The effect of roughness on the contact angle	14
2.2.1 The Wenzel Model	14
2.2.2 The Cassie-Baxter model	16
2.2.3 On roughness	17
2.3 Material properties	19
2.3.1 Elastomeric Polydimethylsiloxane, PDMS	19
2.3.2 Copper	21
2.3.3 Ferric Chloride, $Fe(III)Cl_3$	21
2.3.4 1H, 1H, 2H, 2H-Perfluorodecanethiol	22
2.3.5 SU-8 series photoresist	22
2.4 Photolithography	22

2.5	Characterization	25
2.5.1	Scanning Electron Microscope (SEM)	25
2.5.2	Atomic Force Microscope (AFM)	29
2.5.3	Contact stylus profilometry	32
2.5.4	Contact angle measurements	33
3	Methods	35
3.1	PDMS replication	36
3.2	Etched copper as a PDMS mold	36
3.2.1	Phololithography of Replicated PMDS	38
3.2.2	Gold deposition and lift-off	38
3.2.3	1H,1H,2H,2H-Perfluorodecanethiol treatment of the gold-patterned PDMS surface	38
3.3	Sandpapers as a PDMS molds	39
3.4	Photoresist-patterned sandpaper as a PDMS mold	39
3.5	Replicating PDMS from PDMS	40
3.5.1	Hydroxypolymethylcellulose (HPMC)	40
3.5.2	Trichloro(1H,1H,2H,2H-perfluorooctyl)silane	40
3.6	Characterization	42
3.6.1	Scanning Electron Microscope (SEM)	42
3.6.2	Atomic Force Microscope(AFM)	42
3.6.3	Stylus Profilometer	43
3.6.4	Contact Angle Measurements	43
4	Results	45
4.1	PDMS replicated from etched copper plate	46
4.2	PDMS replicated from sandpapers	46
4.3	PDMS replicated from SU-8 patterned sandpaper	47
4.4	PDMS replicated from PDMS	52
4.4.1	Hydroxypolymethylcellulose (HPMC)	52
4.4.2	Trichloro(1H,1H,2H,2H-perfluorooctyl)silane	52

<i>CONTENTS</i>	ix
5 Discussion	59
5.1 Etched copper as PDMS mold	59
5.2 Sandpapers as PDMS molds	60
5.3 SU-8 patterned sandpaper as PDMS mold	62
5.4 PDMS replicated from PDMS	63
5.4.1 Hydroxypolymethylcellulose (HPMC)	63
5.4.2 Trichloro(1H,1H,2H,2H-perfluorooctyl)silane	64
6 Conclusion	67
Bibliography	75

List of Figures

1.1	Illustration of different ways of micropatterning a surface by a) photolithography(the pink layer on top of the surface is the photoresist, details of the method described in theory section 2.4)[3] ,b)laser beam etching [4] and c)chemical surface modification[5]. The photolithography can be used for etching, lift-off or as a mold.	5
1.2	The self cleaning properties of the lotus leaf: Dirt is removed from the surface as water droplets rolls over it.[6]	6
1.3	SEM images of lotus leaf at different magnifications [7].	6
2.1	The sum of intermolecular forces on a molecule at a liquid surface is directed in towards the bulk. [8]	10
2.2	a)The surface tensions of the solid-vapor, solid-liquid and liquid-vapor interfaces, γ_{sv} , γ_{sl} and γ_{lv} , and the contact angle θ that can be derived from Young's equation (2.2)[9] and b)illustration of the imagined movement of the TPL giving Young's equation for a droplet in equilibrium.	11
2.3	a) The advancing, θ_a , receding, θ_r and the tilting angle, α_t [9]. The tilting angle at which the surface needs to be tilted for a drop to roll off is proportional to the contact angle hysteresis, $\Delta\theta$ and b) The relationship between the advancing contact angle(\circ) and receding contact angle(\bullet) and the roughness of the surface. This is from an experiment where telomer waxes have been sprayed on a flat glass surface, and where made smoother and smoother by successive heat treatments. The roughness scale is qualitative only. [10]	13
2.4	The Wenzel contact angle as a function of roughness at five different contact angles at smooth surfaces.	15
2.5	The two models on contact angles on rough surfaces, the Wenzel model and the Cassie-Baxter model. [2]	15
2.6	All of these profiles have the same R_a value, but are widely different in shape and spacing [11].	17

2.7	The probability density functions for a) different skewness and b) different kurtosis at zero skewness. [11]	18
2.8	An illustration of the profiles of a rough surface at different skewness and kurtosis. The figure is a modification of a figure from [11].	19
2.9	The molecular structure of PDMS. A silicon-oxygen backbone surrounded by methyl groups. [12]	19
2.10	The reaction of the components of the base and curing agent for PDMS into cross-linked PDMS. 1) siloxane oligomers terminated with vinyl groups and 2) cross-linking siloxane oligomers. [13]	20
2.11	The formula for 1H, 1H, 2H, 2H-Perfluorodecanethiol [14].	22
2.12	The chemical formula of Bisphenol A Novolak epoxy oligomer used in SU-8. [15]	23
2.13	Positive resists become soluble upon exposure while negative resists, such as the SU-8 series, become insoluble upon exposure.	24
2.14	A setup for a scanning electron microscope. [16]	26
2.15	SE will only escape from areas close to the surface, the amount depending on the topography of the surface.	27
2.16	The interaction volume of an electron beam with the sample in SEM. The different parts of the volume give rise to different signals [17].	27
2.17	Gas molecules, M , collide with electron beam and create positive ions, $+$, and electrons, e . The positive ions can be neutralized by the excess electrons on the surface, $-$. [18]	28
2.18	a) The deflection of the AFM cantilever is detected by a laser beam reflected off the top of the cantilever, via a mirror, to a photodiode sensor. b) A setup for using tapping mode on the AFM.	30
2.19	The Force experienced by the AFM tip as a function of the tip's distance to the surface. The part of the graph that is underneath the dotted line ($F=0$) is where the tip experiences attractive force to the surface. The part of the graph over the dotted line is where the tip experiences repulsive forces to the surface [19].	30
2.20	The acquired image from AFM of a sample with a high height-to-width ratio may be more describing of the AFM tip than the sample itself [20].	31

2.21	The difference between a normal, sharp tip, a dual tip and a dull tip is illustrated. The dual tip will make features of the surface appear several times in the image, while the dull tip will make features on the surface appear more rounded off than they are and decrease the resolution of the image.	32
2.22	The trace of the stylus tip is dependent on the stylus' radius.[21] . .	33
3.1	The steps of PDMS fabrication. The base and hardener are mixed at a 10:1 relationship for a couple of minutes, degassed, poured into the mold, degassed again, cured and peeled off the mold. This illustration was remade from [22]	37
3.2	The fabrication of a PDMS surface with a rough surface with smooth pillars. The PDMS replication of a SU-8 patterned sandpaper followed by silanization of this PDMS surface, and another PDMS replication with the silanized PDMS as a mold.	41
3.3	The tip and cantilever of the MPP-11100 probes from Bruker[23] . .	43
3.4	An image illustrating the setting of the baseline and the area in which you find the drop[24].	44
4.1	a) The PDMS made from the copper plate mold shows little roughness at x1k magnification in the SEM. The white spot in the image is a place that was zoomed in on earlier, and is an effect of poor conductance on the surface and b) The gold patterned surface after lift-off. The gold-free circles are $\sim 450\mu m$ in diameter.	47
4.2	The difference in contact angle of the PDMS surface is due to the difference in roughness of the molds: a)Buehler ltd's special emery grinding paper with the grit number P1000, b)Sandpaper Nr 4/0, 30331, Schmirgelpapier Blau Deutsches Erzeugnis, Germania and c)Norton's P600 Paper Sheet T489.	48
4.3	SEM images of a PDMS surface replicated from Buehler ltd's special emery grinding paper with the grit number P1000 at 100, 1,000 and 10,000 magnification.	49
4.4	AFM image of PDMS replicated from Buehler ltd's special emery grinding paper with the grit number P1000. The image was made using tapping mode.	50
4.5	The profilometer graphs from the same replication of sandpaper into PDMS. The red and green pillars are markers, and not a part of the result.	51

4.6	The profilometer result from a)SU-8 patterned sandpaper with $400\mu m$ pillars and b-c)the PDMS replicas of this surface. The red and green pillars are markers, and not a part of the result.	53
4.7	The PDMS surface produced from a SU-8 patterned sandpaper with pillars $\sim 1mm$ in diameter. The rough surface with smooth wells is depicted after a)being submerged in water and b)being firstly wetted by ethanol, then submerged in water.	54
4.8	SEM images of the PDMS structure with flat pillars. This is replicated from HPMC treated PDMS with wells. This again, was replicated from the sandpaper-SU-8 mold with SU-8 pillars $400\mu m$ in diameter.	55
4.9	SEM images of the a)smooth well of the PDMS replicated from SU-8 patterned sandpaper and b)the smooth pillar of the PDMS replicated from the silanized PDMS replicated from SU-8 patterned sandpaper. The well/pillar is approximately $1mm$ in diameter.	57
4.10	These SEM images illustrate the roughness of the a)PDMS replicated from SU-8 patterned sandpaper and b)the PDMS replication of the silanized PDMS.	58
4.11	The images taken with CAM200 for the curve fitting and contact angle calculations of water droplets on a) a PDMS surface replicated from sandpaper and b) a PDMS surface replicated from a silanized PDMS surface replicated from sandpaper.	58

CHAPTER 1

Introduction

Lately, advances in medicine, biology and pharmacy has lead to an increase in the number of compounds that may be used as a drug, the drug candidates. In order to filter out the most promising compounds, a high-throughput analysis of the candidates would be helpful.

High-throughput screening is the screening of chemical libraries consisting of thousands of compounds. These are screened in an assay for different purposes. This can be the high-throughput toxicity screening of drug candidates [25], the screening for novel antibacterials [26] or the screening of the transcription dynamics in cells [27]. Compared to the chemical compounds used in biological systems, the number of possible chemical compounds to be used in biological systems are many times bigger [28]. This makes for a lot of drug candidates, e.g. from combinatorial chemistry[29] or diversity-oriented synthesis [30].

The conventional method of cell culturing and analysis use relatively big wells(for example the Greiner Bio-One Microplates: 96 half-area well plates with wells of 5 mm in diameter and a volume per well of $199\mu\text{l}$ and 384 Small Volume TM plates has wells of diameter 1,84–3,3 mm and a volume per well of $28\mu\text{l}$ [31].). Each of these wells are exposed to different compounds, at different concentrations. More cells, culturing media and culturing material than necessary are used, and the big plate assays take up space in the culturing chamber. In high-throughput screening 10,000 to 100,000 chemical compounds are screened in a biological assay [28].

In the analysis of cells different responses are monitored. This could be e.g. the cells viability [25], expression of proteins [32], expression of genes [33], migration [34], proliferation [35, 36] and differentiation[37, 38]. In order to determine these changes in the cell, different techniques are used such as fluorescence microscopy [39, 38, 27], flow cytometry [35] and Western blotting assay(for protein concentration) [35].

To make the in vitro analysis valid for in vivo, the in vitro assay need to be made to mimic the cells' surroundings in vivo [4]. In addition, the cells used for such

experiments are often cancerous cell lines, and will behave differently than the healthy cells in vivo [32]. For this purpose, human stem cells are being developed to screen for e.g. blood system disorders [40].

Different micropatterning techniques can be used in the development of high-throughput drug/toxic screening arrays, such as

- photolithography and lift-off [41, 3], figure 1.1a
- laser/electron beam etching [4]
- chemical surface modification [5]

Topography/roughness, biochemistry and chemical motifs, surface wettability, surface charge, functional groups and mechanical properties, like stiffness all interfere with protein adsorption and cell attachment [5] and can be used to control cell attachment.

In this project, the use of a superhydrophobic and non-superhydrophobic patterned surface is proposed as a way to isolate cells in small areas. In order to make this work, superhydrophobic areas on the surface are needed. This can be achieved either by controlling the surface chemistry or the surface roughness on a hydrophobic material. The former can be realized by silanisation with an apolar silane, deposition of a fluoropolymer on the surface, ultra violet O_3 (UVO) radiation and more [42, 5].

Rough surfaces are known to create superhydrophobicity in surfaces with hydrophobic properties. One of the inspirations behind artificial, superhydrophobic surfaces is the lotus leaf, figure 1.2. The wax covered leaf has structures, both micro and nano scale, figure 1.3. When rain falls on the leaf, it will make droplets with contact angles $>150^\circ$. These will roll off the leaf at angles above 5° , taking dirt with them. The use of roughness of a hydrophobic surface has been explored, using both nano and micro structures [43, 44]. Ranging from polydimethylsiloxane (PDMS) microstructures from simple SU-8 molds [43] to triple-scale roughness of Poly(methyl methacrylate) (PMMA) [45] to a one-step casting process of polystyrene (PS) [46]. Many materials are used, and the means of fabrication vary as well.

The potential of an artificial material with the same properties as the lotus leaf is huge. Self-cleaning, de-icing, anti-icing and non-fogging materials, used for e.g. self-cleaning window frames and solar cells are only some of the possibilities [7, 42].

Patterned superhydrophobic and non-superhydrophobic surfaces leave the latter areas less hydrophobic, and more easily wettable than the former. The idea is

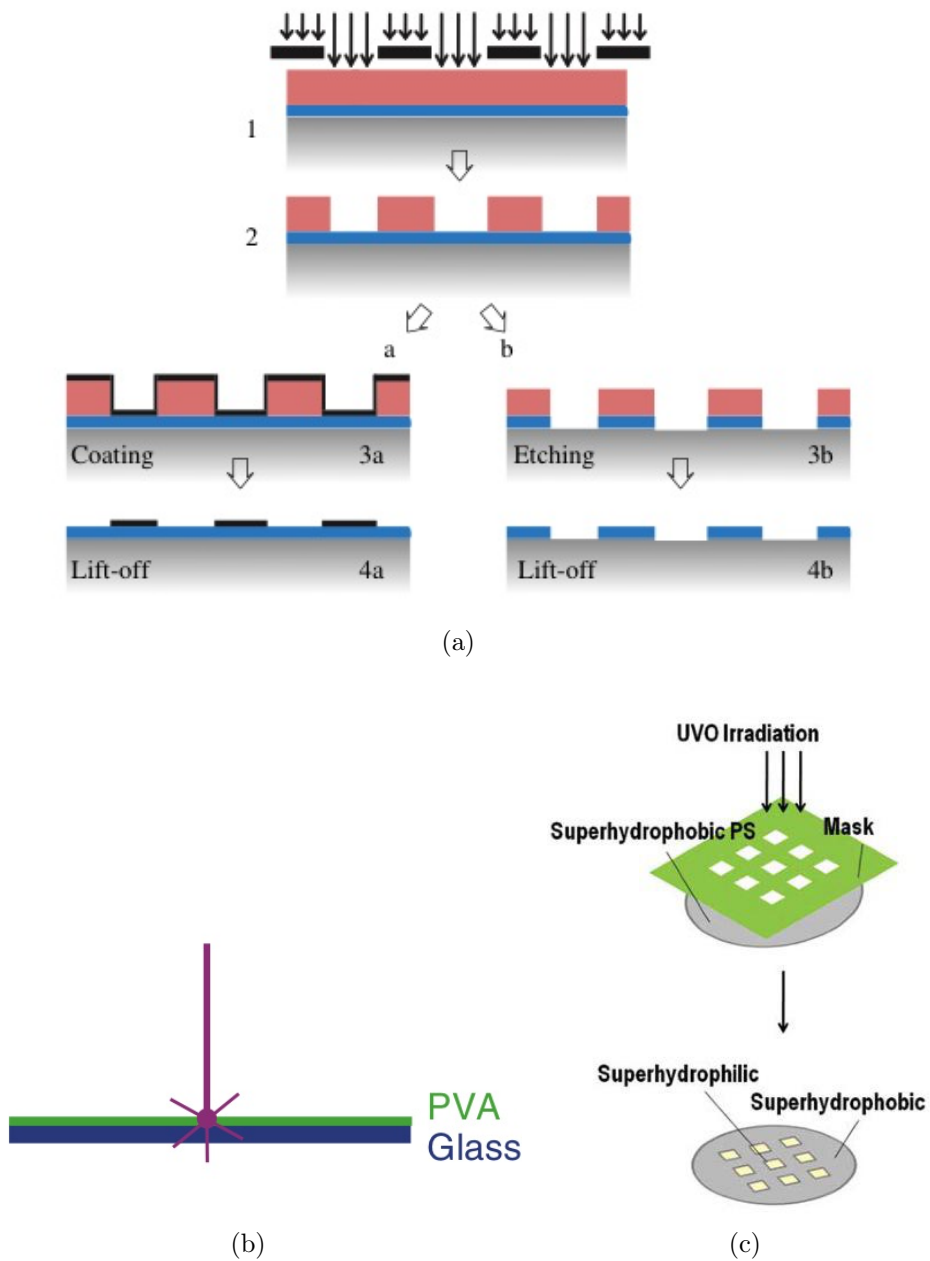


Figure 1.1: Illustration of different ways of micropatterning a surface by a) photolithography (the pink layer on top of the surface is the photoresist, details of the method described in theory section 2.4) [3], b) laser beam etching [4] and c) chemical surface modification [5]. The photolithography can be used for etching, lift-off or as a mold.



Figure 1.2: The self cleaning properties of the lotus leaf: Dirt is removed from the surface as water droplets rolls over it.[6]

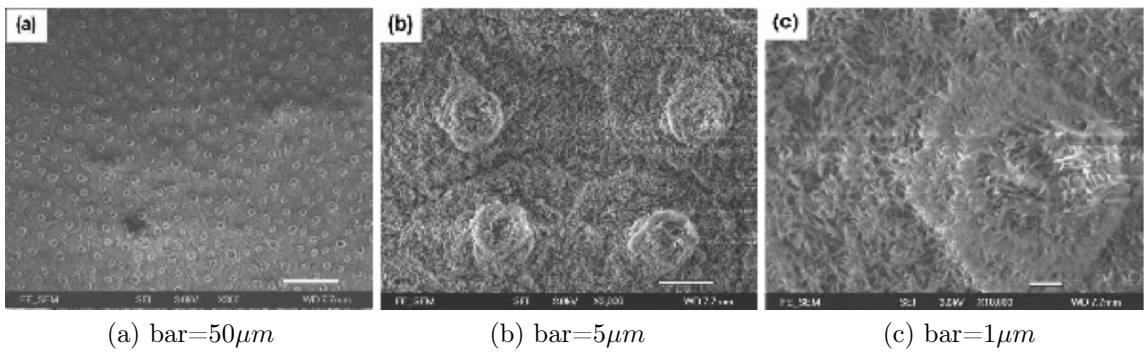


Figure 1.3: SEM images of lotus leaf at different magnifications [7].

that you can use such surfaces to isolate water or water-based solutions on the less hydrophobic areas. The optimal would be if you can dip your surface in liquid, and end up with liquid in predictable amounts in the assigned areas, and no other places on the surface. This project aims at creating a surface where this is achieved solely by different roughness in the different areas. Such a surface would be produced very easily (by the molding of PDMS into an appropriate mold).

The enhancement of hydrophobicity is only possible on an already hydrophobic surface. The least hydrophobic areas will still be hydrophobic and will still dislike water. It might therefore be slightly optimistic to believe that the goal of water capturing in these areas will be achieved by this method. If the less hydrophobic areas were hydrophilic instead, the water capturing to these areas would be more achievable, but this is not possible solely by changing the roughness of the surface. This will be explained thoroughly in the theory part.

Fabrication of spheres and half-spheres [47], open microfluidic devices [48] and controlling cell attachment [5] are some of the applications. The latter can be combined with the biofunctionalization of the non-superhydrophobic areas.

This thesis will look at the use of patterned PDMS surfaces with smooth areas on an otherwise rough surface. The hypothesis is that this surface can capture cell containing droplets in the smooth areas only, thereby capture the cells on the surface in an ordered manner, and at a certain volume (dependent on the size of the smooth areas). The ideal deposition of droplets onto the smooth areas would be by dipping of the entire surface in the cell containing suspension. The project will also look at ways to produce superhydrophobic surfaces by inexpensive and easy means.

CHAPTER 2

Theory

Contents

2.1	Contact Angle and Hydrophobicity	10
2.1.1	Contact Angle Hysteresis	12
2.2	The effect of roughness on the contact angle	14
2.2.1	The Wenzel Model	14
2.2.2	The Cassie-Baxter model	16
2.2.3	On roughness	17
2.3	Material properties	19
2.3.1	Elastomeric Polydimethylsiloxane, PDMS	19
2.3.2	Copper	21
2.3.3	Ferric Chloride, $Fe(III)Cl_3$	21
2.3.4	1H, 1H, 2H, 2H-Perfluorodecanethiol	22
2.3.5	SU-8 series photoresist	22
2.4	Photolithography	22
2.5	Characterization	25
2.5.1	Scanning Electron Microscope (SEM)	25
2.5.2	Atomic Force Microscope (AFM)	29
2.5.3	Contact stylus profilometry	32
2.5.4	Contact angle measurements	33

This project is mainly on the use of roughness to manipulate the contact angle of a surface. Therefore, an understanding of both contact angles is needed to understand the results. Also, the theory on roughness and the effect of roughness on the contact angle explained by two different models is necessary. Some information on certain important materials is added to increase the understanding, together with theory on the characterization methods used to obtain the results.

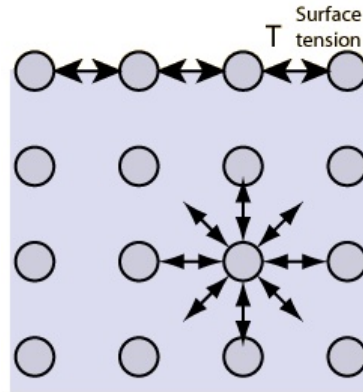


Figure 2.1: The sum of intermolecular forces on a molecule at a liquid surface is directed in towards the bulk. [8]

2.1 Contact Angle and Hydrophobicity

A droplet deposited on a surface will spread until it reaches its equilibrium. At this point, it may wet the surface at different degrees. The degree of wetting is described by the liquid's angle to the surface, the contact angle θ , figure 2.2a.

To understand why the droplet will have this exact angle at a flat surface at equilibrium, one has to look at surface energy. At the interface between two phases a contracting force exists to minimize the surface area between the two phases. The surface tension [N/m] is a measure of this force, the force required to expand the interface area.

The reason behind this effect is found at the molecular level. In a liquid's bulk phase, molecules are symmetrically surrounded by other molecules whose attractive and repulsive forces sum up to zero. At the surface of a liquid-gas interface, however, the mean powers on the molecules are directed inwards, where all the rest of the molecules are. The gas molecules are of lower density than the molecules of the liquid phase, and are considered to be too few and too far away to have any effect [49]. This means that the intermolecular powers at the surface will act to contract the surface, making the surface area as small as possible. The driving force towards equilibrium is the reduction of energy in the system, and the energy can be described by the Gibbs free energy, G .

When a droplet is deposited on a surface, it will move to equilibrium, and achieve a contact angle θ . There are three interfaces and three corresponding interfacial surface tensions (see figure 2.2a) are involved: solid-vapor (γ_{sv}), solid-liquid (γ_{sl}) and liquid-vapor (γ_{lv}).

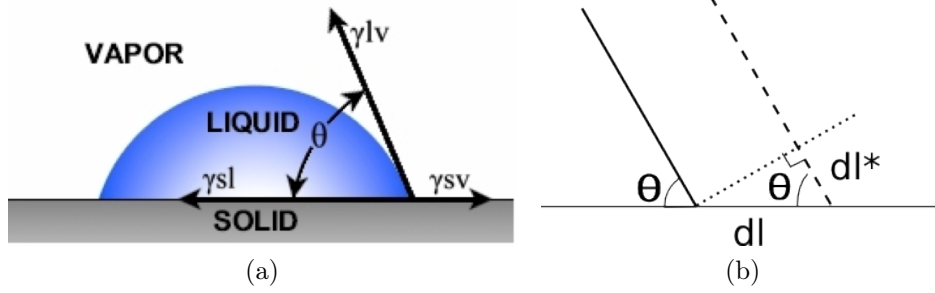


Figure 2.2: a) The surface tensions of the solid-vapor, solid-liquid and liquid-vapor interfaces, γ_{sv} , γ_{sl} and γ_{lv} , and the contact angle θ that can be derived from Young's equation (2.2)[9] and b) illustration of the imagined movement of the TPL giving Young's equation for a droplet in equilibrium.

The line where the three interphases meet, the line that meets the surface and gives us the contact angle, is called the *three-phase line* (TPL). At the equilibrium contact angle, the total surface free energy, described by Gibbs free energy, will not change if the TPL is moved by an infinitesimal length dl to the right. Considering the changes in area to the three interfaces at an imagined plane going into and out of the paper in contact with all three interfaces. The change in area is explained by a unit length l . The total change in interfacial energy can thus be described by

$$dG = \gamma_{sl}l(dl) + \gamma_{lv}l(dl^*) - \gamma_{sv}l(dl) \quad (2.1)$$

From figure 2.2b, the relation $dl^* = dl \cos \theta$ can be derived. Being at equilibrium, $dG=0$, and (2.1) can be simplified to Young's equation [50]

$$\cos \theta = \frac{\gamma_{sv} - \gamma_{sl}}{\gamma_{lv}} \quad (2.2)$$

For a hydrophobic surface, the contact angle of water on the smooth solid is $\theta > 90^\circ$, and for a hydrophilic surface, the contact angle is $\theta < 90^\circ$. From Young's equation it is evident that the contact angle of 90° marks the change where the surface tension of the interfaces solid-vapor and liquid-vapor are equal. For hydrophobic surfaces, the surface tension from the solid-vapor interface is smaller than that of the liquid-vapor interface. The opposite is true for hydrophilic surfaces.

The contact angle of water on a surface is dependent on the chemical and physical (described in following sections). For a flat surface, it is the chemical properties of the surface that determine its properties.

The effect of a hydrophobic surface on water is similar to that of the water with the vapor. Hydrophobic, non-polar surfaces will not create hydrogen bonds to the water. The water "looses" hydrogen bonds and prefer not to be in contact with the water. A hydrophilic surface will generally be polar, and capable of hydrogen bonding [51].

2.1.1 Contact Angle Hysteresis

Another measure on contact angle is the advancing and receding contact angles, θ_a and θ_r that explains how the liquid behave if the droplet is filled with water or if water is removed from a droplet that has reached equilibrium. If you add water to the droplet, the solid-liquid interface area will stay the same, while the contact angle increases, until you pass a certain contact angle, the advancing contact angle, θ_a , and the solid-liquid interface increases in area.

If you on the other hand remove water from the droplet, typically with a syringe, the solid-liquid interface will stay the same while the contact angle decreases, until you pass a the receding contact angle, θ_r , and the solid-liquid interface decreases in area.

The difference in the advancing and the receding contact angles is called the contact angle hysteresis

$$\Delta\theta = \theta_a - \theta_r \quad (2.3)$$

and is a measure on how easily a droplet will roll of, figure 2.3a, or stick to, a surface.

The definition of a superhydrophobic surface is a contact angle above 150° , but another way of determining it is by a low contact angle hysteresis. The contact angle hysteresis is proportional to the tilting angle at which the surface needs to be tilted for a drop to roll off the surface [52],

$$\alpha_t \propto \Delta\theta \quad (2.4)$$

To sum up, a superhydrophobic surface has a high contact angle, $\theta > 150^\circ$, and will therefore have a small solid-liquid interface area with hydrophilic liquids. Droplets on the surface will also roll off the surface at low angles due to a low contact angle hysteresis, $\Delta\theta$. These two properties might be in competition, as the contact angle hysteresis relates to the roughness according to figure 2.3b.

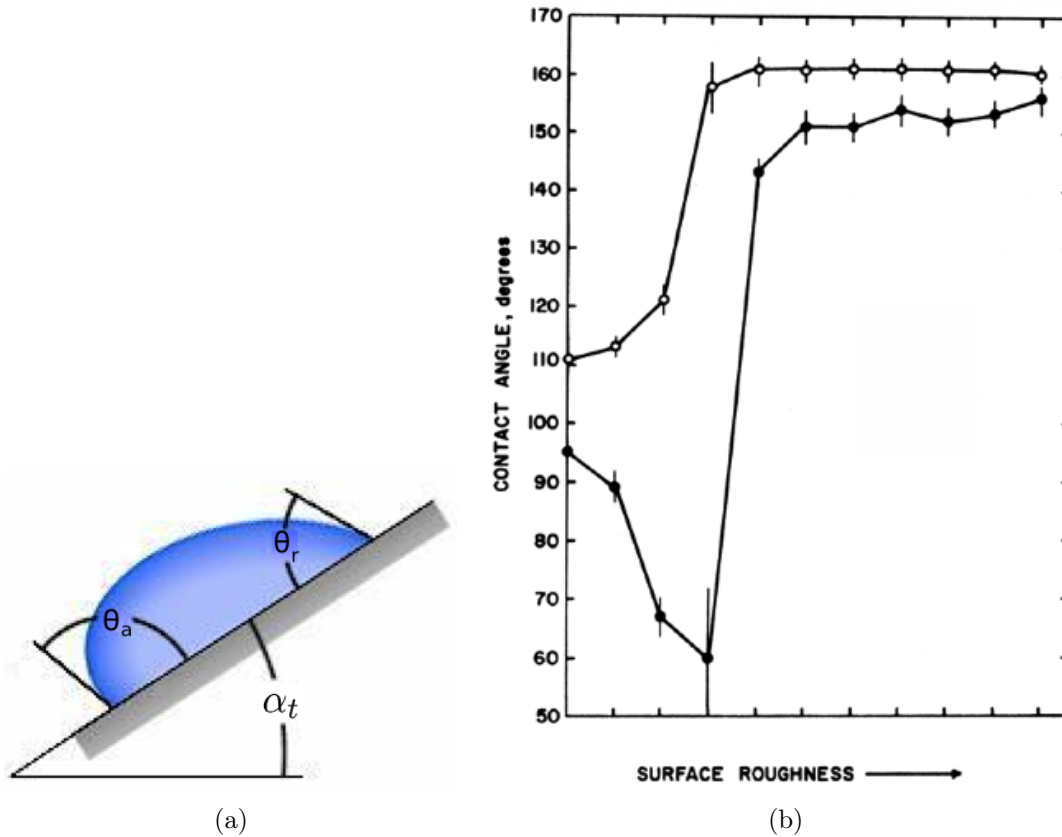


Figure 2.3: a) The advancing, θ_a , receding, θ_r and the tilting angle, α_t [9]. The tilting angle at which the surface needs to be tilted for a drop to roll off is proportional to the contact angle hysteresis, $\Delta\theta$ and b) The relationship between the advancing contact angle(○) and receding contact angle(●) and the roughness of the surface. This is from an experiment where telomer waxes have been sprayed on a flat glass surface, and where made smoother and smoother by successive heat treatments. The roughness scale is qualitative only. [10]

2.2 *The effect of roughness on the contact angle*

So far, the contact angle on a flat, homogenous surface has been explained. For rough surfaces, however, Young's model is not valid. This is explained by two different models, the Wenzel model and the Cassie-Baxter model. The first explains the difference in contact angle on a rough surface by the increased interfacial area on a rough surface. The other, the Cassie-Baxter model, explain the differences by trapped gas bubbles in the valleys of the roughness, that the water really is not in contact with the underlying surface, but with gas.

Both of the models for rough materials are conceptual models and can not be identified in practice[53]. They do however, explain how surfaces can reach a higher contact angle than that of the highest observed contact angle on flat surfaces with solid-liquid-vapor interfaces, which is about 120° [10].

2.2.1 *The Wenzel Model*

In 1936 the contact angle on a rough surface was described by Robert N. Wenzel by introducing a roughness factor, r_w

$$r_w = \frac{\text{true surface area}}{\text{geometric surface area}} \quad (2.5)$$

where the geometric surface area is the area the droplet seems to cover when watched from above. He integrated this roughness factor into Young's equation(2.2) to form the Wenzel equation

$$r_w(\gamma_{sv} - \gamma_{sl}) = \gamma_{lv}\cos\theta_w \quad (2.6)$$

The Wenzel contact angle, θ_w , figure 2.5a, can be expressed by the contact angle for a flat material and the roughness factor:

$$\cos\theta_w = r_w\cos\theta \quad (2.7)$$

The Wenzel equation (2.6) will have a different outcome from Young's equation depending on the contact angle for the flat material. For hydrophobic materials, the Wenzel contact angle will be bigger than Young's contact angle, while it for hydrophilic materials will be lower than young's contact angle. To what degree this happens is described in figure 2.4

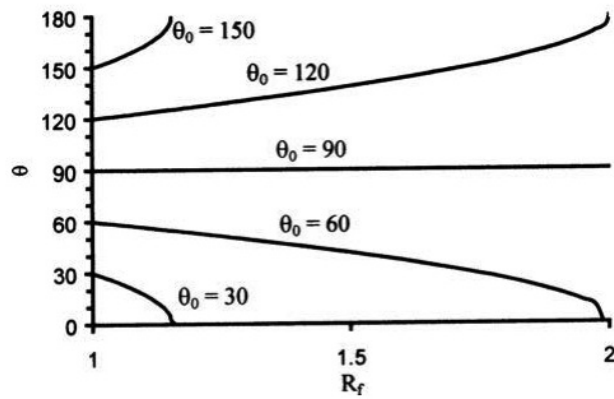


Figure 2.4: The Wenzel contact angle as a function of roughness at five different contact angles at smooth surfaces.

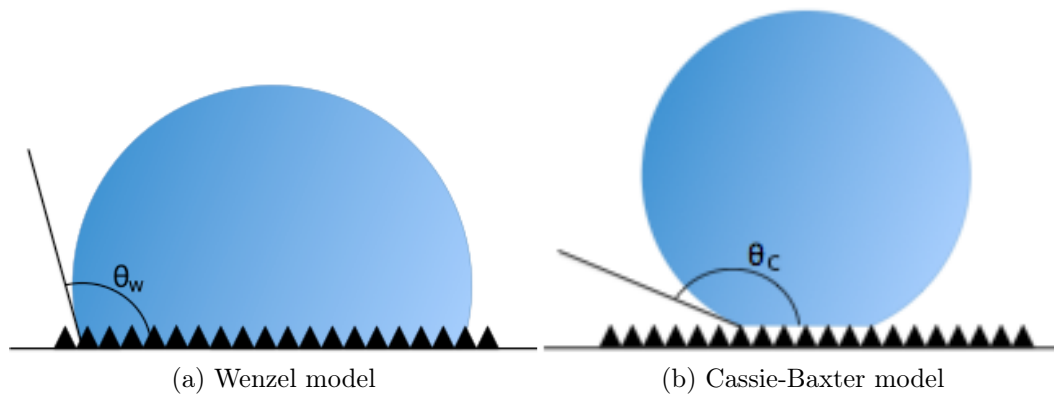


Figure 2.5: The two models on contact angles on rough surfaces, the Wenzel model and the Cassie-Baxter model. [2]

2.2.2 The Cassie-Baxter model

A drawback with the Wenzel model is that it does not take into account that all of the surface may not be wetted by the liquid. In fact, the part that is not wetted can be considered to be another type of interface. For a droplet with a flat underside on a surface of different materials, the difference between γ_{sv} and γ_{sl} equals

$$\gamma_{sv} - \gamma_{sl} = \sum_1^n a_i(\gamma_{i,sv} - \gamma_{i,sl}) \quad (2.8)$$

for the surface of fractions $a_1, a_2 \dots a_n$. Inserted into Young's equation (2.2), the Cassie-Baxter contact angle can be expressed by [54]

$$\cos\theta_c = \frac{1}{\gamma_{lv}} \sum_1^n a_i(\gamma_{i,sv} - \gamma_{i,sl}) \quad (2.9)$$

For a rough surface, there will be two fractions, one for the solid, and one for the vapor trapped under the drop, 2.5b. The resulting equation

$$\cos\theta_c = \frac{a_1(\gamma_{1,sv} - \gamma_{1,sl}) + a_2(\gamma_{2,sv} - \gamma_{2,sl})}{\gamma_{lv}} \quad (2.10)$$

can be further simplified by considering that in the case of vapor as a second fraction, $\gamma_{2,sv} = 0$ (the surface tension of a vapor-vapor interface) and $\gamma_{2,sl} = \gamma_{lv}$:

$$\cos\theta_c = \frac{a_1(\gamma_{1,sv} - \gamma_{1,sl})}{\gamma_{lv}} - a_2 \quad (2.11)$$

This means that the Cassie-Baxter angle can be calculated from the fraction of vapor and the fraction of solid in contact with the flat underside of the flat droplet together with the contact angle of the same, smooth solid:

$$\cos\theta_c = a_1 \cos\theta - a_2 \quad (2.12)$$

Finding the fractions a_1 and a_2 might be quite a challenge, although this may be calculated if you assume that the Cassie-Baxter model is descriptive of your system, and use a measured contact angle. However, it is more likely that the droplet on the surface is explained partly by Wenzel, partly by Cassie-Baxter. In addition, it is very unlikely that a real droplet will be totally flat over the vapor, as the Cassie-Baxter model assumes.

2.2.3 On roughness

Roughness can be defined by Wenzel's roughness factor, r_w , equation 2.7. However, this is a huge simplification. The roughness is local minima and maxima of different amplitudes and at different spacings. The roughness can be described by the mean of the absolute deviations in height over the entire surface from the mean height of the surface, R_a :

$$R_a = \frac{1}{L} \int_0^L |z - m| dx \quad (2.13)$$

with a variable height z from a reference line on the analyzed distance L over which the mean height m is given by:

$$m = \frac{1}{L} \int_0^L z dx \quad (2.14)$$

This expression do not explain the shape and spacing of the surface features, and figure 2.6 illustrates how different surfaces with the same R_a can be. The variance of the height difference over the surface is given by

$$\sigma^2 = \frac{1}{L} \int_0^L (z - m)^2 dx \quad (2.15)$$

$$= R_q^2 - m^2 \quad (2.16)$$

where R_q is

$$R_q = \frac{1}{L} \int_0^L (z^2) dx \quad (2.17)$$

From equation 2.15 it is obvious that $\sigma = R_q$ when $m = 0$. That is to say, if the reference line is defined at the mean height.

The skewness(Sk) and the kurtosis(K),

$$Sk = \frac{1}{\sigma^3 L} \int_{-\infty}^{\infty} (z - m)^3 dx \quad (2.18)$$

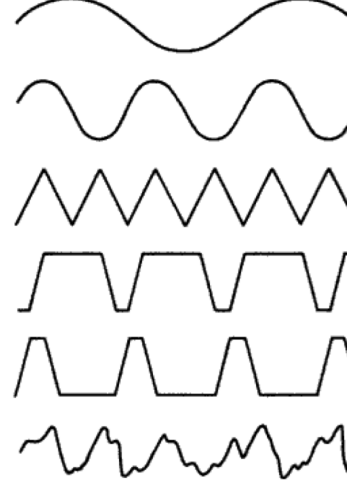


Figure 2.6: All of these profiles have the same R_a value, but are widely different in shape and spacing [11].

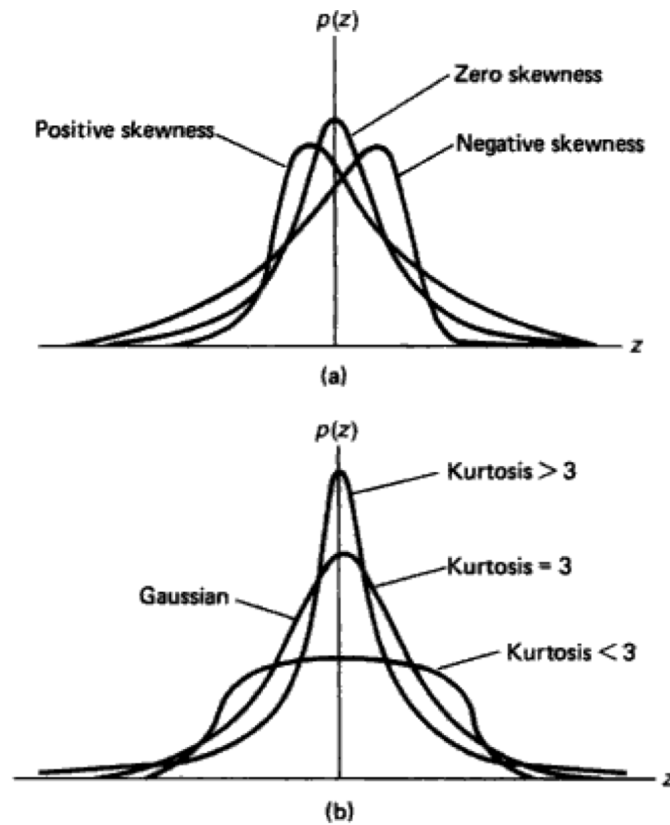


Figure 2.7: The probability density functions for a) different skewness and b) different kurtosis at zero skewness. [11]

$$K = \frac{1}{\sigma^4 L} \int_{-\infty}^{\infty} (z - m)^4 dx \quad (2.19)$$

are means of explaining the symmetry and shape of the roughness.

The skewness is a number on the symmetry of the density function, figure 2.7a. If the peaks are blunt, the skewness is negative, if they are sharp, the skewness is positive and if the surface structure has valleys as sharp/blunt as the peaks, the skewness is zero, figure 2.8.

The kurtosis is a number on the sharpness of the peaks and valleys. If the kurtosis value is 3 and the skewness is zero, you have a Gaussian probability density function. If the kurtosis is > 3 , the peaks and valleys are sharper than those of the gaussian function, while a kurtosis of < 3 indicates that the valleys and peaks are blunter than those of the gaussian distribution.

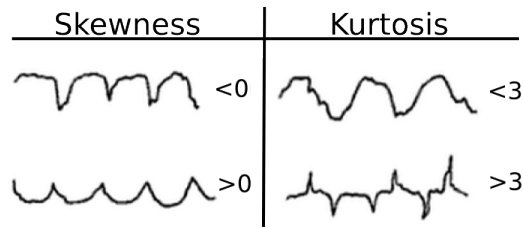


Figure 2.8: An illustration of the profiles of a rough surface at different skewness and kurtosis. The figure is a modification of a figure from [11].

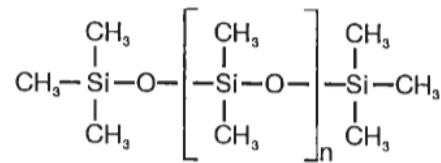


Figure 2.9: The molecular structure of PDMS. A silicon-oxygen backbone surrounded by methyl groups. [12]

2.3 Material properties

2.3.1 Elastomeric Polydimethylsiloxane, PDMS

Elastomeric Polydimethylsiloxane (PDMS), or silicone, is a transparent (down to 280nm wavelength), nontoxic and elastic plastic. This makes it good, and widely used, for the analysis of cells [22, 55, 56, 57].

The structure of PDMS is illustrated in figure 2.9. It has a silicon-oxygen backbone and arms in the form of methyl groups. PDMS can reproduce structures at very low scale, and is widely used within the field of soft lithography. One of the reasons for this is that the PDMS cures at low temperatures ($-45^\circ\text{C} - 200^\circ\text{C}$), and can incorporate proteins and other substances that might be ruined at higher temperatures.

The contact angle of PDMS is $101.8 \pm 3.4^\circ$ [2] on flat surfaces, but PDMS can also be made hydrophilic by plasma treatment. It is enough to put the PDMS in a oxygen plasma chamber for approximately 15 seconds at 100–150 W and <0.05 Torr. This will incorporate oxygen atoms in the surface, so that $-\text{OH}$ groups protrude from the surface and makes it hydrophilic.

Making a PDMS replica from a mold you start by mixing a base and a curing agent at a ratio given by the producer. This is stirred for several minutes and degassed in a vacuum chamber to remove the bubbles that arise from the mixing.

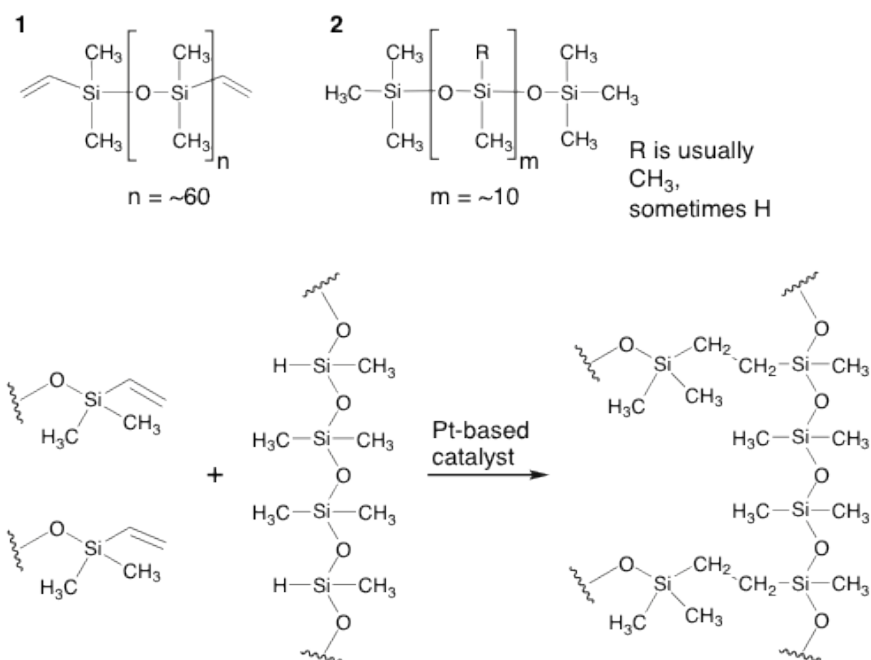


Figure 2.10: The reaction of the components of the base and curing agent for PDMS into cross-linked PDMS. 1) siloxane oligomers terminated with vinyl groups and 2) cross-linking siloxane oligomers. [13]

The mix is poured into the mold and cured.

The base component consists of siloxane oligomers terminated with vinyl groups, figure 2.10-1 and a platinum-based catalyst. The curing agent consists of the same siloxane oligomers terminated with vinyl groups and of cross-linking siloxane oligomers, figure 2.10-2, with two or more silicon-hydride bonds. The platinum-based catalyst of the base cures the elastomer by an organometallic cross-linking reaction [13]. The Si-H bonds of the cross-linking siloxane oligomers add to the double bonds of the siloxane oligomers terminated with vinyl groups and form $\text{Si} - \text{CH}_2 - \text{CH}_2 - \text{Si}$ linkages.

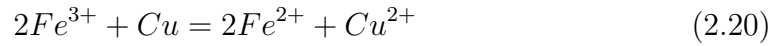
Because of the many reaction sites of the cross-linking siloxane oligomers, three dimensional cross-linking can happen. The reaction does not have waste products, and the temperature will accelerate the cross-linking. The PDMS cures at different temperatures, but the curing time will be longer for lower temperatures.

2.3.2 Copper

Solid copper can be either single crystals, which are very difficult to produce, or polycrystalline. In a crystal structure, the atoms are perfectly arranged in a lattice. Single crystals have one such lattice for all of the atoms, while a polycrystal contain many smaller crystals stuck together in a somewhat random way [58]. The boundary between these crystals are called grain boundaries.

2.3.3 Ferric Chloride, $Fe(III)Cl_3$

The etching effect of ferric chloride, $Fe(III)Cl_3 \cdot 6H_2O$, has been investigated by [59]. The ferric ions reacts with copper to form cupric ions [60]:



This is a method that is diffusion limited, and the production of Cu^{2+} is proportional to the amount of Fe^{3+} within the diffusion barrier film of a thickness δ . The concentration change over time for the two ions can be calculated by[61]

$$\frac{dc}{dt} = \frac{D_{Cu^{2+}}A(c_1 - c)}{\delta V} \quad (2.21)$$

$$\frac{da}{dt} = \frac{D_{Fe^{3+}}A(a_1 - a)}{\delta V} \quad (2.22)$$

where c is the concentration of Cu^{2+} , c_1 is the concentration of Cu^{2+} at the copper surface, $D_{Cu^{2+}}$ the diffusion constant of Cu^{2+} in $FeCl_3$ solution, A is the area of the copper sheet and V is the volume of the etching solution. For equation (2.22) a is the concentration of Fe^{3+} , a_1 is the concentration of Fe^{3+} at the copper surface and $D_{Fe^{3+}}$ the diffusion constant of Fe^{3+} in $FeCl_3$ solution.

This means that the rate of copper etching depends on the area of etching, the volume of the etchant, the diffusion constant of the different ions, the thickness of the diffusion barrier film and the concentration at the etching surface. The rate of the reaction will be impossible to determine by these equations without knowing δ , a_1 or c_1 .

The copper atoms at the grain boundaries, see subsection 2.3.2, are more loosely bound than the copper atoms in the rest of the crystal, and will be the first to react with an etchant. Also, the different orientations render the copper atoms at the surface bound to the rest of the atoms to a varying degree. This will lead to the copper being etched at different rates over the surface, making valleys at the grain boundaries and hills in the middle of the copper crystal(or grain). The effect will vary for different etching solutions, and is not well documented for $Fe(III)Cl_3 \cdot 6H_2O$ in an approximately neutral solution.

2.3.4 1H, 1H, 2H, 2H-Perfluorodecanethiol

Perfluorodecanethiol is a molecule that can form self-assembled monolayers(SAMs) in a very thin film. The film is superhydrophobic with a water contact angle of 163° and contact angle hysteresis of less than 3° [62].

Thiol groups are adsorbed onto gold, silver, copper, palladium, platinum and mercury [63]. The chemical structure of 1H, 1H, 2H, 2H-Perfluorodecanethiol is illustrated in figure 2.11. The thiol(-SH) group is able to adhere to certain metals, while the hydrogen-free fluorocarbon tail is highly hydrophobic.

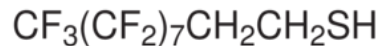


Figure 2.11: The formula for 1H, 1H, 2H, 2H-Perfluorodecanethiol [14].

2.3.5 SU-8 series photoresist

SU-8 is an epoxy based, negative photoresist. It is developed for high aspect ratio patterns, like MEMS e.g.. [64]. It also allows for a relatively thick layer of photoresist on a surface. The thickness of a photoresist is dependent on the spinning conditions during the spin coating, but also the viscosity of the photoresist.

SU-8 uses the resin Bisphenol A Novolak epoxy oligomer, figure 2.12. This has 8 epoxy functionalities that are reactive and cross-link after the photoactivation by i-line exposure[15]. The i-line exposure decompose the photoacid generator, triarylsulfonium hexafluoroantimonate salt, into hexafluoroantimonic acid. This will in turn protonate the epoxides of the Novolak epoxy. During post exposure bake, the protonated oxonium ions react with the neutral epoxides to form cross-links.

The SU-8 series has resists of different viscosity, and are named accordingly. A SU-8 5 photoresist, at 290 cSt viscosity [65], is far less viscous than the SU-8 2000 series, with SU-8 2015 at 1250 cSt viscosity[66]. The SU-8 300 series, however, do not follow the same naming pattern, and is actually less viscous than the SU-8 2000 series. The SU-8 series can produce photoresist layers from 0, $5\mu\text{m}$ to $550\mu\text{m}$.

2.4 Photolithography

Photolithography is a technique extensively used in semiconductor technology. It is the printing of temporary circuit structures by a photoresist that assist etching

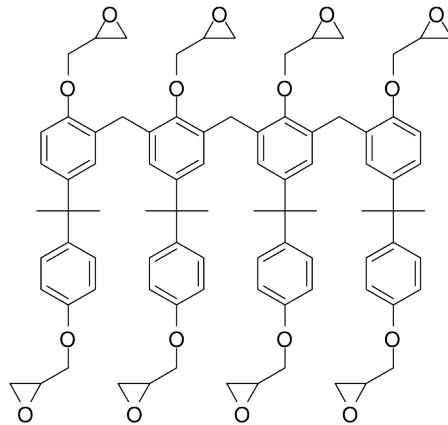


Figure 2.12: The chemical formula of Bisphenol A Novolak epoxy oligomer used in SU-8. [15]

and deposition processes[67]. You can say it acts as a shield to certain parts of the surface that is not to be exposed to the following processes. After these processes are finished, the photoresist can be removed by a solvent and, in the case of previous deposition, "lift-off" of the material deposited on the resist. Thus, leave a pattern of the deposited material, or etched surface, in the areas that was not covered by the photoresist.

Conventional photoresists are photo-sensitive materials that are suitable for manipulation at the i-line UV wavelengths, 365 nm. The resists are made up of resin, sensitizer, solvent and, in some cases, additives. The photoresists can be divided into two categories: Negative i-line photoresists and positive i-line photoresists.

Negative photoresists(e.g. SU-8) are resists that will become less soluble upon exposure to UV light. One of the resins used in negative photoresists may be the Bisphenol A Novolak epoxy oligomer of SU-8 or chemically inert, natural rubber [67]. The sensitizer for the negative photoresists is a photoactive agent that releases nitrogen gas when it is exposed to i-line UV light. This generates free radicals that will cross-link the resin molecules. The cross-linked photoresist will now be insoluble in the developer solution, while the non-exposed areas of the photoresist will be dissolved by this solution.

Positive photoresists, like negative photoresists, contain resins (e.g. *novolak*, a phenol-formaldehyde polymer). The sensitizer in positive resists is a photoactive compound that upon i-line UV exposure goes from being a dissolution inhibitor to being a dissolution promoter. At development, the photoresist that was exposed will be dissolved, while the non-exposed photoresist will stay.

So, in order to get a good photoresist pattern, you need a good mask to shield the

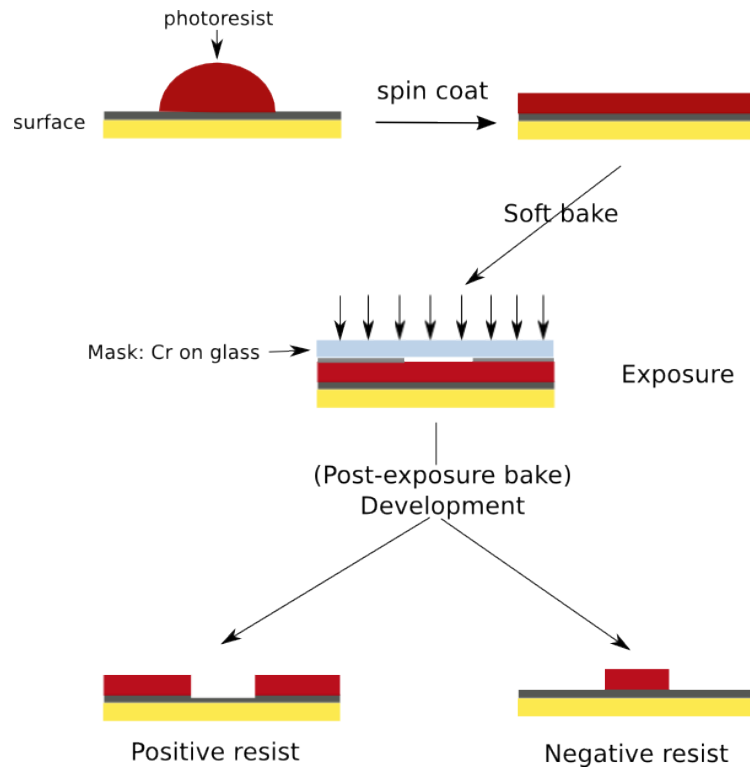


Figure 2.13: Positive resists become soluble upon exposure while negative resists, such as the SU-8 series, become insoluble upon exposure.

parts of the photoresist that should not be exposed to the UV light. The design of such a mask will depend on whether you use a negative or a positive resist, see figure 2.13. The design can be made in a software such as CleWin and be printed onto a mask. For good resolution, a mask of chromium on a glass slide can be made.

Before exposure, the photoresist is spread evenly on the wafer/surface by spin-coating. The properties of the resist and the choice of spinning parameters determine the thickness of the resist. After the spin-coating, the resist-covered sample is soft baked. This is to remove the solvents from the polymer and improve its adhesion to the surface and its uniformity. After cooling, the mask is aligned on the resist-covered sample. Depending on the type of resist, the thickness of the resist and the reflective properties of the underlying material, the exposure dosage of UV light, [Jm^{-1}], is determined.

After exposure, the resist is developed by dissolving the soluble areas of the resist by a developing solution. The development leaves only the desired pattern of resist. For some resists, hard bake might be necessary to remove residual solvent, harden

the resist and improve the adhesion before the development. This is not done for all resists.

Inspecting the developed pattern of resist is the final step. This can be done optically to ensure that the resist looks like the pattern, and has not been overdeveloped, overexposed, underdeveloped or underexposed.

2.5 Characterization

2.5.1 Scanning Electron Microscope (SEM)

The Scanning electron microscope (SEM) is a tool that is used when the required resolution goes beyond that of the optical microscope, which has a limit of about $0,2 \mu\text{m}$ resolution[68]. SEM, on the other hand, can achieve a xy resolution below 10nm. The SEM uses electrons as a probe that scans the surface. The electrons interact with the surface and several different signals can be obtained from the scan. These signals come from different parts of the sample, as illustrated in figure 2.16.

The electrons of the electron beam are generated by an electron gun and are directed, accelerated and focused into a beam that focuses on the sample, see figure 2.14. This will be impossible in air, because the gas molecules of the air will scatter the electrons and decrease the resolution and signal.

Therefore, this process is managed at a vacuum, and the sample must be able to withstand the pressure change from atmospheric pressure to that of the SEM so that it is not altered before imaging. Another restriction of the SEM is that the sample surface must be conductive, so that the electrons do not accumulate on the surface and give signals to the detectors from a wider area than the area that are being scanned. These signals can be considered as noise, and will make your image worse. The electrons might also damage non-conductive sample with a build-up of electrons at the surface.

The microscope can create images from the signal of both backscattered electrons and from secondary electrons. The backscattered electrons originate from the electron beam and interacts inelastically with the sample, while the secondary electrons are electrons from the surface that has been emitted due to interaction with the electron beam.

For investigating the topography of a surface, the signals from the secondary electrons can be used. These are loosely bound electrons from specimen atoms that have been emitted as a result of the electron beam's ionization of the atoms. The

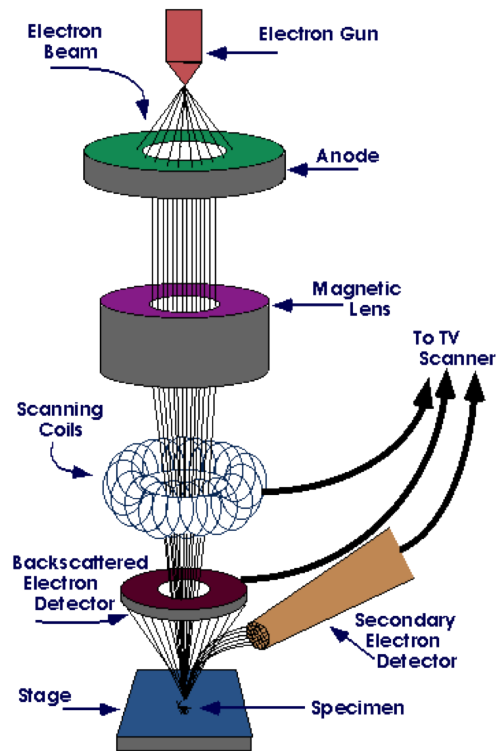


Figure 2.14: A setup for a scanning electron microscope. [16]

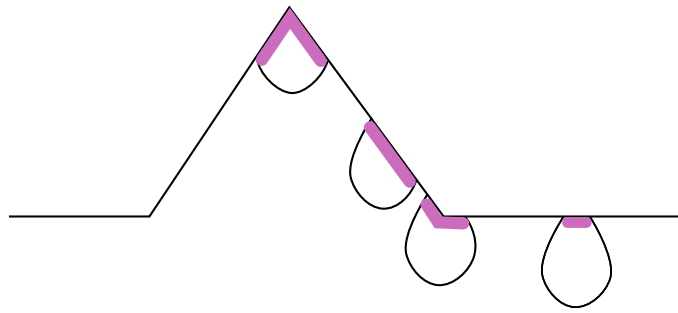


Figure 2.15: SE will only escape from areas close to the surface, the amount depending on the topography of the surface.

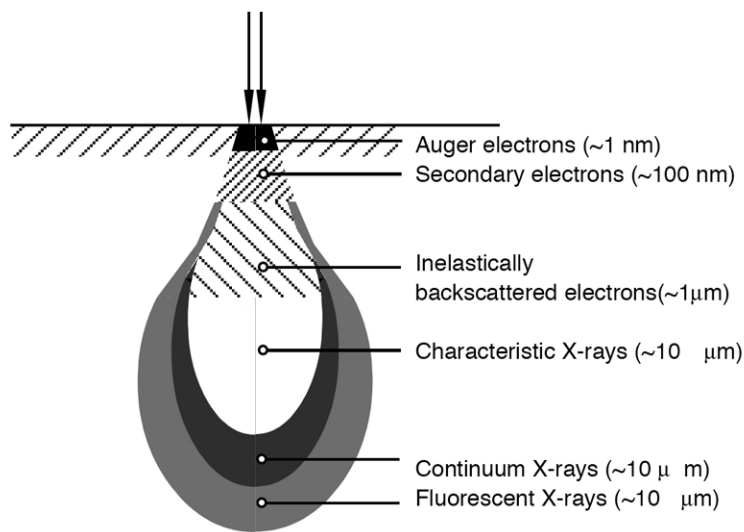


Figure 2.16: The interaction volume of an electron beam with the sample in SEM. The different parts of the volume give rise to different signals [17].

secondary electrons have energies less than 50 eV[69], and can only escape if they are emitted within a few nanometers from the surface. This results in a change in signal from the secondary electrons depending on the topography of the sample, figure 2.15. The signal will be greater when there is a feature on the surface, than when the surface is flat.

Backscattered electrons(BSE) are electrons that originate from the electron beam and are electrons of high energy that are deflected off the surface of the sample. On average they have 60% – 80% of the initial energy of the electrons. The BSEs are electrons that have interacted with the atoms of the sample in elastic scattering interactions, and are affected by the atom numbers of the atoms they interacted with. Thus, the BSE signal contains information on the composition of the sample.

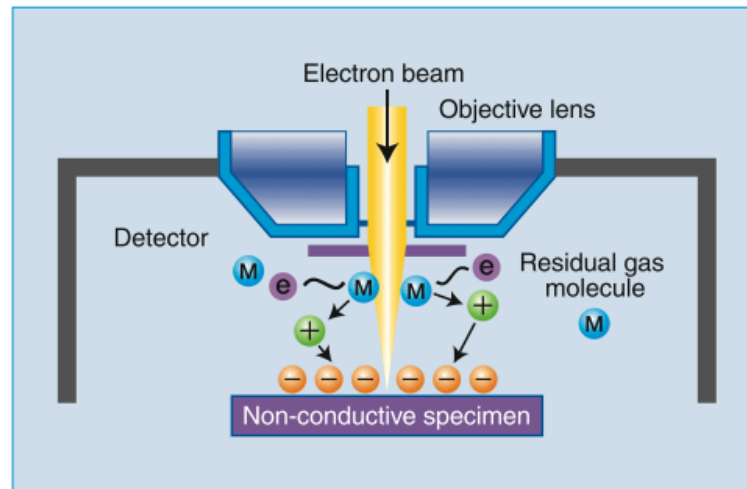


Figure 2.17: Gas molecules, M , collide with electron beam and create positive ions, $+$, and electrons, e . The positive ions can be neutralized by the excess electrons on the surface, $-$. [18]

The heavier elements will scatter back more electrons than the lighter ones, making them appear brighter in the produced image. From figure 2.16 it is obvious that the BSE arise from a greater volume of the sample, which in turn will result in poorer resolution for a BSE produced image compared to that of a SE produced image.

Even though the BSE contains information on the composition of the sample, the use of several BSE detectors, can give a good image of the topography of the surface [70]

Low-Vacuum SEM

Low vacuum SEMs are scanning electron microscopes with a higher pressure than regular SEMs in the chamber containing sample, electron gun, anodes, lenses, scanning coils and detectors when the sample is being scanned. The pressures are greater than pressures greater than 10 Pa [71], while regular SEMs have pressures of typically 10^{-4} Pa [72]. Low-Vacuum SEMs are microscopes made for biological samples, which are not conductive.

At low vacuum, the electrons that at higher vacuum would build up on the surface, will be transferred to positive ions generated from electron beam interaction with gas molecules, figure 2.17. This will decrease the charge-up effect on the sample and make better images for non-conductive samples.

Sputter Coater

As a pretreatment to the SEM imaging of a non-conductive sample, a layer of conductive metal can be deposited on the surface of the sample. This will give a better contrast in pictures, and charge-up at the surface will be avoided. A sputter coater is a means to deposit such a layer.

The sputter coater is an instrument that evacuates air from the specimen chamber and fill argon gas into it. A voltage is subsequently put over a cathode and anode in the chamber, and a glow discharge of the argon gas occurs. This will result in ion bombardment of the cathode.

In the sputter coater, the cathode is made up of the material you want to coat your sample with, the target(of the ion bombardment). When this is bombarded with ions, it will erode, and metal atoms from the target are sputtered in all directions, including towards your sample, that is placed on the anode in the specimen chamber. The sputter coater can by different means estimate the thickness of the sputtered layer, and you can set the machine to sputter a certain thickness of metal onto your sample [73].

2.5.2 Atomic Force Microscope (AFM)

While the SEM is a great technique to get an idea on the structure of a surface, it can not measure the height differences over this surface. Atomic force microscopy (AFM) is a good instrument for this purpose.

The AFM consists of a tip, situated on a cantilever, a detection system, a scanning system and a feedback system, see figure 2.18b. This is a probing technique where a fine tip(5-10 nm radius is commercially available) is scanned over the surface of the sample while the tip's interaction with the sample is monitored.

The AFM tip is positioned on a cantilever, and will experience a force when it is close to the surface, figure 2.19, that will go from being attractive to repulsive as the tip approaches the surface, and will affect the deflection of the cantilever. The deflection of the cantilever is determined by a laser beam that is directed to the top of the cantilever and is reflected off the cantilever via a mirror to a photodetector, figure 2.18a.

The tip can probe the surface in different ways, both in contact and in non-contact with the surface, dynamically and statically. For statical operating mode, or contact mode, the AFM the tip is touching the surface at a given, constant force. Any small change in this force is compensated by adjusting the z-position of the sample so that the force stays the same. This way, you get a map on the z-changes over the sample.[20]

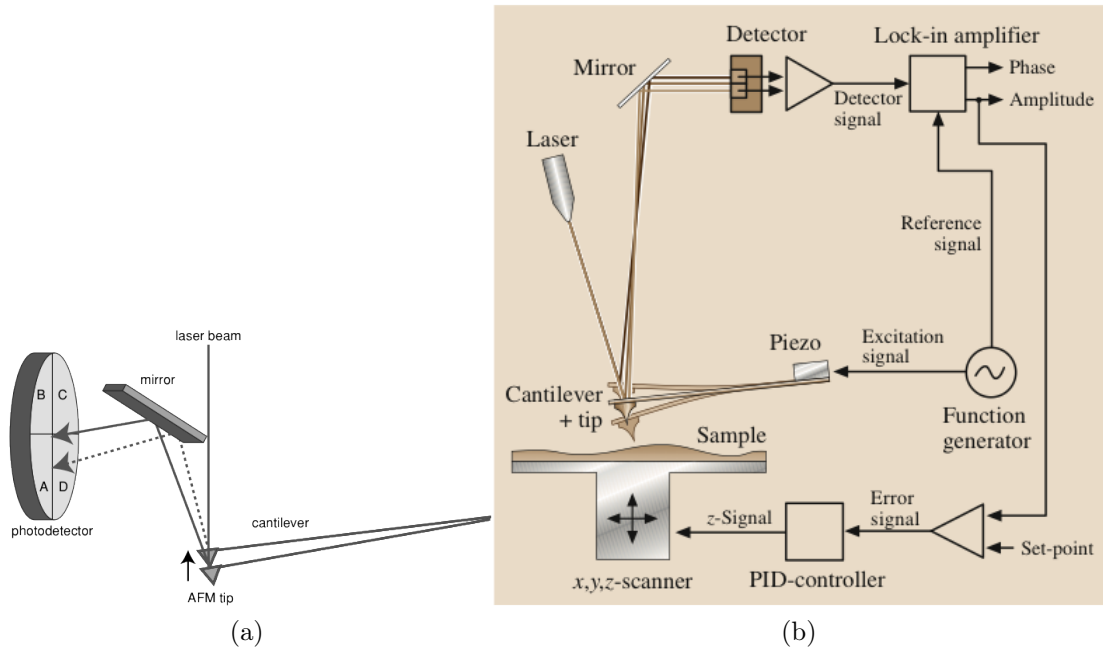


Figure 2.18: a) The deflection of the AFM cantilever is detected by a laser beam reflected off the top of the cantilever, via a mirror, to a photodiode sensor. b) A setup for using tapping mode on the AFM.

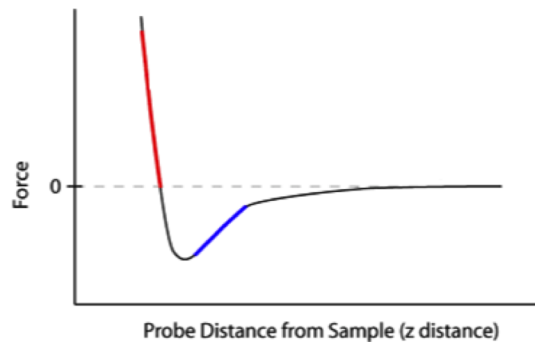


Figure 2.19: The Force experienced by the AFM tip as a function of the tip's distance to the surface. The part of the graph that is underneath the dotted line ($F=0$) is where the tip experiences attractive force to the surface. The part of the graph over the dotted line is where the tip experiences repulsive forces to the surface [19].

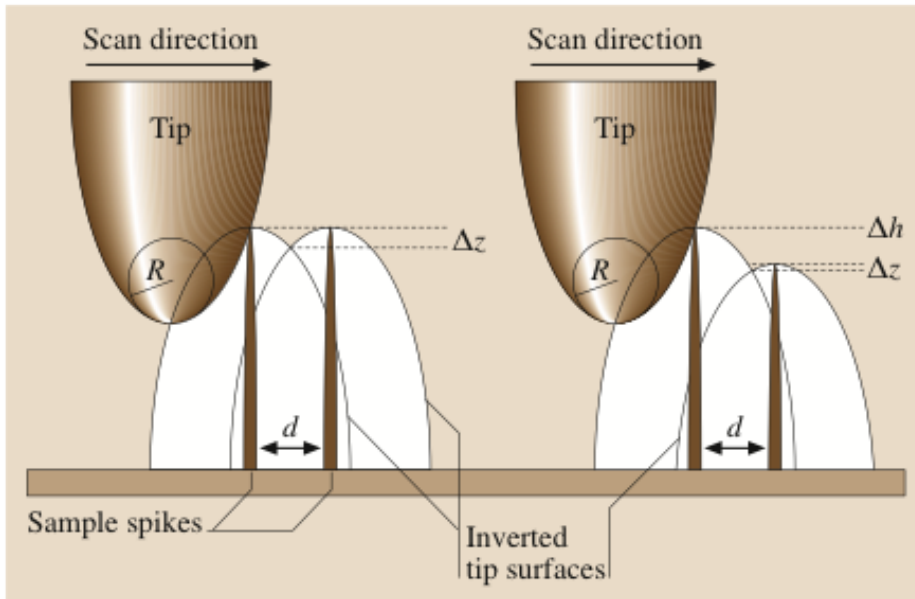


Figure 2.20: The acquired image from AFM of a sample with a high height-to-width ratio may be more describing of the AFM tip than the sample itself [20].

For dynamic operating mode, the tip can both be in contact and non-contact with the surface. If the tip is in contact with the surface in the dynamic mode, it is called tapping mode. In this mode, the cantilever is set to oscillate at a frequency close to the resonance frequency of the cantilever. Figure 2.18b shows one setup for this kind of system. The change of amplitude and phase of the cantilever is recorded, and any change in the amplitude will result in an adjustment of the z-position of the sample by the piezo stage the sample is situated on. It is this change in the z-position over the surface that is recorded and make the picture that is generated by this method.

Another option within the dynamic operating mode is that the AFM tip does not touch the sample at all, non-contact mode. This can be operated with either the amplitude change or the frequency change causing the change in z-position of the sample.

The resolution of an AFM image is highly dependent on the thickness and sharpness of the tip. This is illustrated in figure 2.20. The resolution is dependent on the radius of the tip and the shape of the tip. A long, thin tip will give better resolution than a thicker tip because this will be better able to probe into steep valleys of the sample.

Using the AFM, you can experience problems like dual tips and dull tips. The former is if there is not a single, sharp tip, but a tip consisting of two tips, figure

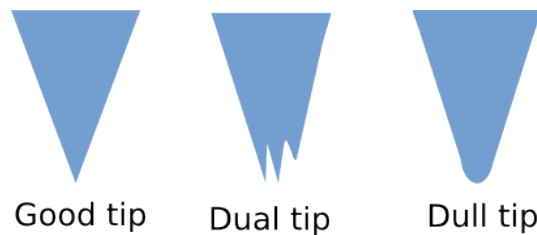


Figure 2.21: The difference between a normal, sharp tip, a dual tip and a dull tip is illustrated. The dual tip will make features of the surface appear several times in the image, while the dull tip will make features on the surface appear more rounded off than they are and decrease the resolution of the image.

2.21, that comes in contact with the sample while scanning. The result is that features on the surface appears two or more times on the picture. Dull tips cause lower resolution and features appear "rounder", figure 2.20, and reflects the shape of the tip more than the shape of the feature. The shape and size of the tip is determining the resolution of the scan.

The AFM is a technique that is good for measuring height differences and getting a picture of the topology. Also, if you for some reason do not want to coat your non-conductive, the AFM is a good option. A drawback is that the AFM cannot measure big samples, big differences in height, determined by the shape and size of the tip and cantilever. Depending on the x,y,z-scanner, figure 2.18b, the AFM is restricted in the total area of each scan/picture. Another drawback is that the method is extremely slow, both getting started and making each picture.

2.5.3 Contact stylus profilometry

The AFM cannot scan larger areas or over high z-differences. For situations where this might be necessary, the contact stylus profilometer can be used. Like AFM, this is a probing technique, but the profilometer has got a different, larger tip and another detection system. For the profilometer, the probe is a stylus on a small arm connected to a piezoelectric element at the other side. A feedback system ensures that the stylus can be brought into contact with the sample at a given force. The piezoelectric element ensures that this force remains constant by adjusting the height of the stylus. The adjustments are recorded and displayed as one line in the final image.

The tip can be of different shapes and sizes, but the radii usually lies between $20\mu m$ and $0.1\mu m$ [74]. The trace of the stylus tip over the surface is dependent on the radius of the tip, figure 2.22. Another restriction of the method is the detection

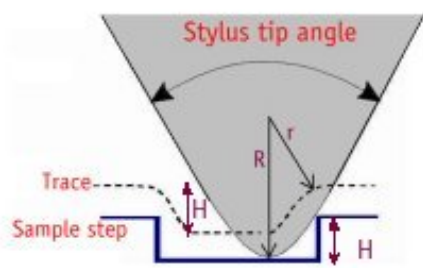


Figure 2.22: The trace of the stylus tip is dependent on the stylus' radius.[21]

system, that is not as sensitive as that of other techniques. The profilometer provides a two-dimensional representation of a sample's micro-structure fast and easily.

The profilometer is sensitive to the height of the surface, and small angles of the surface appear large when you look at height measured in nanometer. The features of the sample may appear bigger/smaller at the beginning of the measurement than at the end. If you have two or more features known to be approximately the same size, the software can readjust the graph so that it mirrors the height differences over the measured line not taking the tilting into account. If you do not have such same height-features on your surface, it becomes really difficult to get large scale differences (you can still look at the difference in height between two adjoined features).

2.5.4 Contact angle measurements

Contact angles (see section 2.1) can be measured in many ways, the most common being the measurement of the static contact angle by looking at the profile of a droplet deposited on surface. This is recorded and analysed to fit the profile of the droplet to the Young-Laplace equation

$$\Delta p = \gamma \left(\frac{1}{R_1} + \frac{1}{R_2} \right) \quad (2.23)$$

giving the change in pressure across the interface of the fluid, Δp , as a function of the surface tension, γ , and the principal radii of curvature, R_1 and R_2 . From this equation, the contact angle of the droplet is calculated.

The tilting plate method and the add-and-remove-volume method measures the advancing and receding contact angles. The former tilts the surface and record the advancing and receding contact angles by looking at the droplet's profile. The

latter adds water to a droplet in equilibrium, and records the advancing angle of the droplet over the surface by analyzing the profile of the droplet. The receding contact angle is measured by this method by the removal of liquid from a droplet in equilibrium and analyzing the receding contact angle from the droplet's profile. The recording, analysis and estimation of the droplet's profile and contact angles can be managed by specialized software [9].

CHAPTER 3

Methods

Contents

3.1	PDMS replication	36
3.2	Etched copper as a PDMS mold	36
3.2.1	Phololithography of Replicated PMDS	38
3.2.2	Gold deposition and lift-off	38
3.2.3	1H,1H,2H,2H-Perfluorodecanethiol treatment of the gold-patterned PDMS surface	38
3.3	Sandpapers as a PDMS molds	39
3.4	Photoresist-patterned sandpaper as a PDMS mold	39
3.5	Replicating PDMS from PDMS	40
3.5.1	Hydroxypolymethylcellulose (HPMC)	40
3.5.2	Trichloro(1H,1H,2H,2H-perfluorooctyl)silane	40
3.6	Characterization	42
3.6.1	Scanning Electron Microscope (SEM)	42
3.6.2	Atomic Force Microscope(AFM)	42
3.6.3	Stylus Profilometer	43
3.6.4	Contact Angle Measurements	43

As previously explained in the introduction, the aim of this project is to make a PDMS surface with patterned rough and smooth areas. The smooth areas are $1mm$ and $\sim 450\mu m$ in diameters(these sizes are a result of available photoresist masks, and the size should be adjusted in further development). This will create a difference in contact angle between the areas, and hopefully allow for the capturing of water in the smooth areas.

The first trial at a rough mold was by the etching of copper. This was explored in a previous project[1], making PDMS with a pretty decent roughness. Another PDMS mold was different sandpapers. One of which was also SU-8 patterned into pillars with smooth tops on a rough sandpaper surface. Thus, the PDMS replicated from this mold had wells with smooth bottoms on a rough PDMS surface.

For PDMS replications from PDMS molds, Hydroxypolymethylcellulose(HPMC) and silanization treatment were explored. The silanization of the PDMS surface with wells in a rough surface was the most successful. The deposition onto the PDMS pillars of Hydroxypolymethylcellulose(HPMC) was also explored.

3.1 PDMS replication

For the PDMS replication, Sylgard 184 silicone elastomer kit, a commercial PDMS from Dow Corning, was used. PDMS base and hardener was mixed at a 10:1 wt% relationship. The viscous mix was stirred for a couple of minutes and treated in a degassing chamber until all visible bubbles were removed.

Next, the mix was poured into a mold made of aluminum foil with the structure to be replicated at the bottom of the mold. The degassing process was repeated in order to remove any bubbles on the surface of the molds. Afterwards, the PDMS was cured in an oven at 100°C for approximately 35 min. Some replications were done overnight at 80°C , but, by far, most replications were cured at 100°C . The whole process is illustrated in figure 3.1.

After the PDMS had cooled down, the aluminum foil was peeled off. The PDMS was then cut into a piece with edges just within those of the replicated structure and peeled off the surface with tweezers.

Etched copper plates(section 3.2), sandpapers(section 3.3) and photoresist-patterned sandpaper(section 3.4) were replicated by PDMS in this study. In addition, the PDMS from sections 3.3 and 3.4 were used as molds and replicated into new PDMS surfaces. This is explained more thoroughly in section 3.5.

3.2 Etched copper as a PDMS mold

The copper used for these experiments were 0.8 mm thick, 6 x8,9 cm polycrystalline copper plates (Polymetaal, The Netherlands). The plates came with a protective layer of plastic. To be sure that this was removed, 2.0M HCl (from Sigma-Aldrich) was used in combination with rubbing with a Q-tip. The copper plates were later rinsed in water and dried off with a pressurized N_2 gun.

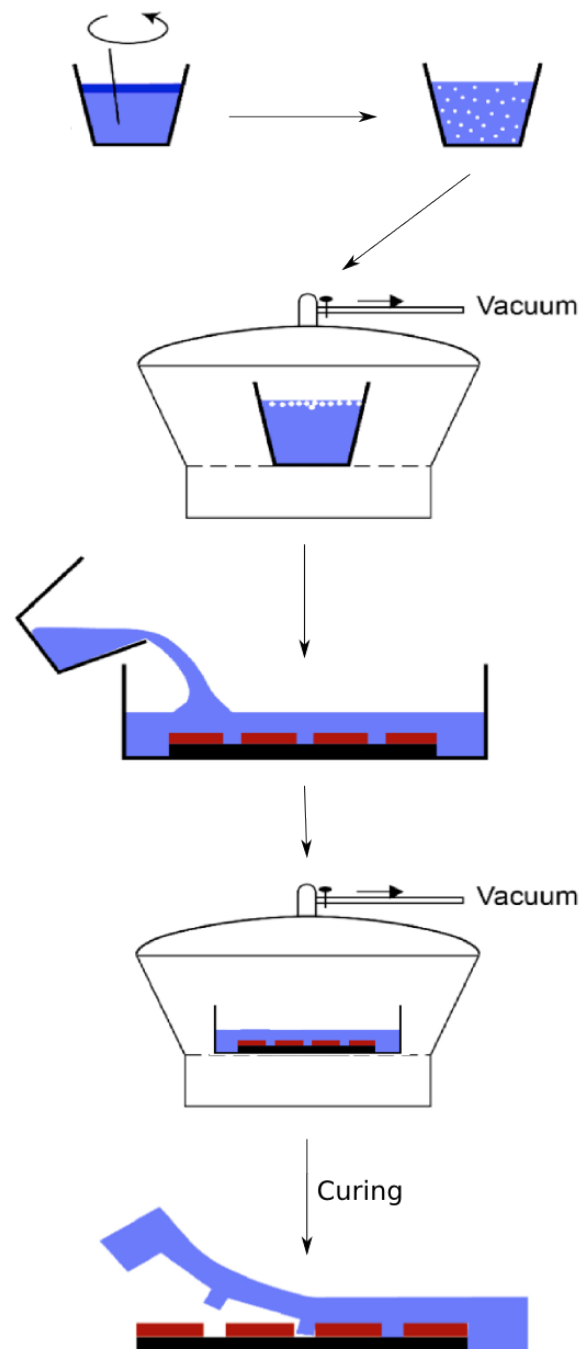


Figure 3.1: The steps of PDMS fabrication. The base and hardener are mixed at a 10:1 relationship for a couple of minutes, degassed, poured into the mold, degassed again, cured and peeled off the mold. This illustration was remade from [22]

The etchant that was used to gain surface roughness was $Fe(III)Cl_3 \cdot 6(H_2O)$, at 0,05M concentration. The copper plates were treated in 100 ml etchant for 20 minutes. Afterwards, they were rinsed thoroughly in water and dried off with N_2 .

The etched copper was used as a mold, and a replica in PDMS was made according to section 3.1.

3.2.1 *Phololithography of Replicated PMDS*

The replicated PDMS was patterned with the ma-n 440 negative photoresist from MicroChem Corp(Massachusetts, USA) after plasma cleaning for 2,5 minutes at 50% oxygen and 50 % power in a Femto plasma cleaner from Diener Electronic.

The photoresist was spun onto the surface at 1000rpm for 30 seconds with 500 rpm/s acceleration. According to the manual, this should give $\sim 7\mu m$ thickness. The photoresist was soft baked for 12 minutes at $95^\circ C$ before it was exposed. The mask used in the exposure was a chromium covered glass plate with circular areas that was not chromium covered. The exposure dose was set to the double of the recommended dose for silicon, which amounted to $2600mJ/cm^2$.

After exposure, the photoresist was developed in the ma-D 332 S developer from MicroChem Corp(Massachusetts, USA) until all the unexposed photoresist was gone ($\sim 2,5$ minutes).

3.2.2 *Gold deposition and lift-off*

A 10 nm thick layer of gold was deposited on the photoresist-patterned PDMS surface by a Cressington 208 HR sputter coater. Afterwards, the photoresist, and the gold layer covering these structures was removed by lift-off in acetone, see figure 1.1a-a. For some samples, this last step was skipped, and the lift-off process was done in the Perfluorodecanethiol solution.

3.2.3 *1H,1H,2H,2H-Perfluorodecanethiol treatment of the gold-patterned PDMS surface*

The gold-patterned PDMS surface was immersed in 1mM 1H,1H,2H,2H-Perfluorodecanethiol in an ethanol solution for 15 minutes. After this, the gold-covered PDMS surface was immersed in 96% ethanol for another 15 minutes.

3.3 Sandpapers as a PDMS molds

The sandpapers that was replicated in this process was

- Buehler ltd's special emery($Al_2O_3 - Fe_3O_4$) grinding paper with the grit number P1000. According to the manufacturer, this has a midpoint in the size of its particles to $8, 2\mu m$ [75].
- Sandpaper Nr 4/0, 30331, Schmirgelpapier Blau Deutsches Erzeugnis, Germania. ¹
- Norton's P600 Paper Sheet T489, with a $25, 8\mu m$ midpoint in the size of its silicon carbide particles.

Pieces of sandpaper were glued onto a glass slide by double sided tape and used as molds in PDMS replication as explained in section 3.1.

3.4 Photoresist-patterned sandpaper as a PDMS mold

A mask made of sandpaper and photoresist was made by depositing SU-8 5 onto the surface of the P1000 special emery grinding paper from Buehler. The SU-8 was spun onto the surface at firstly 500 rpm for 10 seconds with a 200 rpm/s acceleration and then 1500 rpm for 30 seconds with a 200 rpm/s acceleration. This was followed by soft baking at a hotplate set to $65\text{ }^\circ\text{C}$ for one minute and a hotplate set to $95\text{ }^\circ\text{C}$ for 3 minutes.

Inspection of the surface in a light microscope showed the resist layer to be too thin to make an flat surface on top of the sandpaper, and the process was repeated three times.

The surface was exposed to light of 365 nm wavelength through a Karl Suss MJB3 mask aligner. Between the sample and the mercury lamp, a chromium patterned mask was placed chromium-down onto the surface. The exposure was 47 seconds at $9, 6mJ/cm^2s$ intensity.

The photoresist-patterned sand paper was glued onto a glass slide and replicated according to section 3.1. The result was a PDMS replica with a rough surface interrupted by smooth wells.

¹All of the sandpapers were donated from the work shop at NTNU. Unfortunately, the Nr 4/0, 30331, Schmirgelpapier Blau Deutsches Erzeugnis, Germania-sandpaper was probably produced some fifty years ago in Germany, with a numbering system that escapes me. The roughness seem, however, to be somewhere between that of the two others.

3.5 Replicating PDMS from PDMS

To obtain smooth pillars on the surface instead of wells, the replication of PDMS from the already existing PDMS was investigated. This requires some pretreatment of the PDMS-mold. Two such methods were investigated. Firstly, a cellulose polymer, hydroxypolymethylcellulose (HPMC), was deposited on the PDMS as described below, with inspiration and recipe from [76]. Secondly, Trichloro(1H,1H,2H,2H-perfluorooctyl)silane 97% from Sigma-Aldrich was deposited on the surface of the PDMS-mold by a silanization process described in a following section. The result from this last process is illustrated in figure 3.2.

3.5.1 Hydroxypolymethylcellulose (HPMC)

0,5 wt% hydroxypolymethylcellulose(HPMC) was diluted in a 5mM phosphate buffer($NaH_2PO_4 * H_2O$). The phosphate buffer was adjusted to pH 3,07 with HCl before it was mixed with the HPMC.

The first batch was treated with the HPMC-phosphate buffer solution for 10 min before it was removed from the solution and rinsed in deionized water. The surface was dried with pressurized nitrogen gas.

The second batch was dipped in ethanol for $\sim 5seconds$ and then in water for $\sim 30seconds$ before it was treated with the HPMC solution under the same conditions and post-treatments as the previous batch. This was in order to ensure that the entire surface was being treated in the HPMC solution, and that air bubbles on the surface would not hinder this process.

3.5.2 Trichloro(1H,1H,2H,2H-perfluorooctyl)silane

A small amount(using a pipette partly filled by capillary effects) of the liquid was put in a small glass container. This glass container was placed in the bottom of a silanization chamber, and the PDMS-mold on a plastic "shelf" with holes. The silanization chamber is a glass chamber made to facilitate, and keep vacuum. For good working chambers, it would be enough to pump the gas out until vacuum is achieved and then seal the chamber for ~ 1 hr. However, a leaky chamber was used for this project, and the pumping and sealing was repeated at $\sim 5min$ intervals for an hour.

After this process was finished, air was let into the silanization chamber, it was opened, and the sample removed. The PDMS piece was glued by double-sided

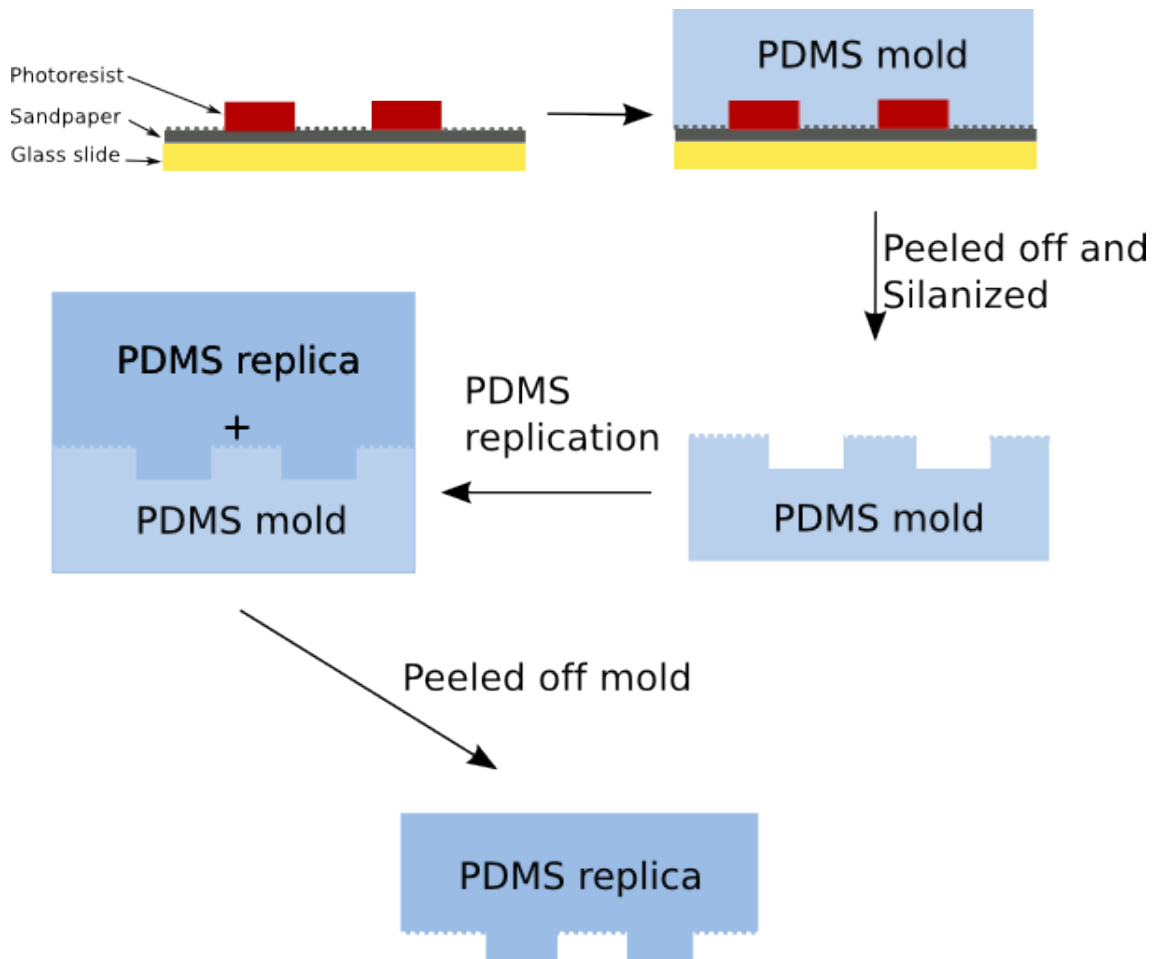


Figure 3.2: The fabrication of a PDMS surface with a rough surface with smooth pillars. The PDMS replication of a SU-8 patterned sandpaper followed by silanization of this PDMS surface, and another PDMS replication with the silanized PDMS as a mold.

tape to a glass slide and a mold of aluminum foil was made around this. The replication of a new PDMS surface was done according to section 3.1.

Hydroxypolymethylcellulose (HPMC) treatment of the pillars of The PDMS replicated by the use of Trichloro(1H,1H,2H,2H-perfluorooctyl)silane

The replicated rough PDMS surface with smooth pillars replicated from the silanized, rough PDMS surface with smooth wells was treated with PDMS on the pillars. A pipette was used to deposit droplets of the HPMC solution on the pillars, and treated for 10 minutes before the surface was rinsed in deionized water and dried with pressurized nitrogen.

3.6 Characterization

3.6.1 Scanning Electron Microscope (SEM)

The characterization with SEM was done using a Hitachi TM3000 tabletop microscope at NTNU NanoLab. This is a low vacuum SEM that is made for biological samples and such, and will reduce the problem of non-conductive samples to a certain degree.

All of the pictures were taken at 15 kV acceleration voltage and fastened with carbon tape to a 23° tilt sample holder. The detection mode used was the COMPO mode. The low conductance samples, e.g. the PDMS samples, were treated with a layer of ~10nm gold coated in a Cressington 208 HR B sputter coater.

3.6.2 Atomic Force Microscope (AFM)

The atomic force microscope at NTNU's NanoLab was used in this project. That is a Veeco dimultimode V AFM, and was used with a J-scanner (~ 160x160 μ m scan size) and the NanoScope730 software.

The tips used in the experiments were MPP-11100 probes from Bruker, 3.3. The height of the tip is 15 – 20 μ m and the mean radius is 8nm (can be up to 12nm) according to the manufacturer [23].

The sample that was to be characterized in the AFM had to be cut into a small, thin shape with a maximum of 15 mm in diameter and 6 mm in height. The sample was glued onto a magnetic sample holder and positioned within the instrument.

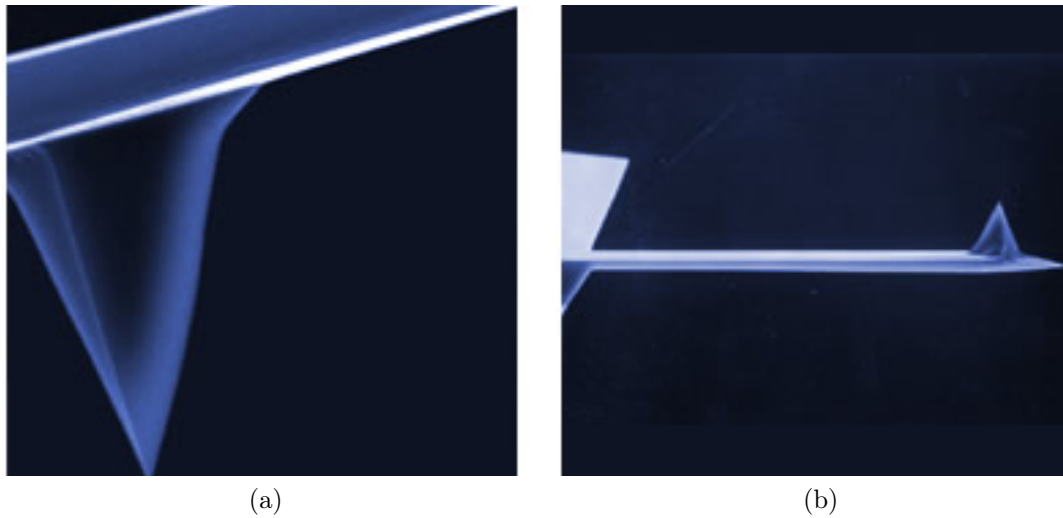


Figure 3.3: The tip and cantilever of the MPP-11100 probes from Bruker[23]

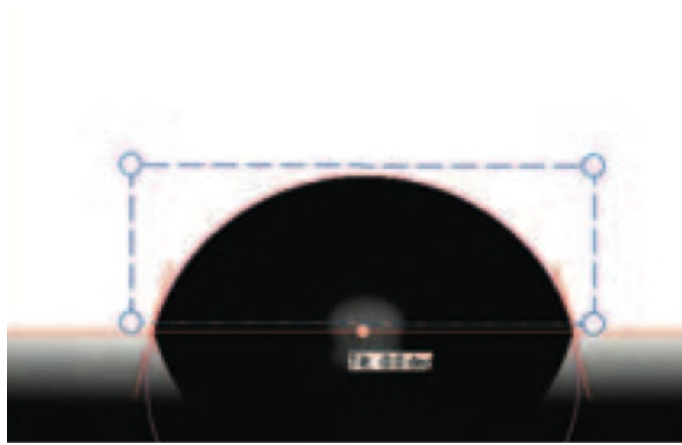
3.6.3 Stylus Profilometer

The Veeco Dektak 150 Profilometer in NTNU's NanoLab was used in these experiments. This has a maximum scan length of 55 mm, a vertical range of $524\mu\text{m}$ and a vertical resolution of 1\AA at the $6, 55\mu\text{m}$ range. The tip installed is a diamond tip stylus with $12.5\mu\text{m}$ in diameter.

3.6.4 Contact Angle Measurements

The contact angle measurement was done with CAM 200, Optical Contact angle meter from KSV instruments ltd. A monochromatic light and a high-resolution CCD camera is used for picture taking of the static drop, which is triggered via the software. In the software, image analysis is performed after defining baseline (e.g. the surface) and the area in which you find the droplet, figure 3.4a.

The surface is placed on the sample stage and a water droplet deposited by a syringe. The images the camera produce is transferred to the software, and the camera is moved so that the focus of the image is on the drop. You then record your picture, define baseline and droplet area in this. The software firstly extract the drop profile before curve fitting this to the Young-Laplace equation. This curve is again used for the calculation of the contact angles on the left and right side of the profile.



(a)

Figure 3.4: An image illustrating the setting of the baseline and the area in which you find the drop[24].

CHAPTER 4

Results

Contents

4.1 PDMS replicated from etched copper plate	46
4.2 PDMS replicated from sandpapers	46
4.3 PDMS replicated from SU-8 patterned sandpaper . . .	47
4.4 PDMS replicated from PDMS	52
4.4.1 Hydroxypolymethylcellulose (HPMC)	52
4.4.2 Trichloro(1H,1H,2H,2H-perfluorooctyl)silane	52

The etched copper plate did not give any great roughness. The gold deposition and Perfluorodecanethiol treatment of the PDMS did not have the desired effect either, and the use of etched copper as a mold was terminated. The PDMS replicas of the three sandpapers had different contact angles, and the contact angle hysteresis of the PDMS from the finest sandpaper was small enough so that a deposited droplet rolled a surface with a small, natural tilt (probably from uneven distribution of the pre-PDMS or a bulky mold).

The finest sandpaper had a contact angle of $162, 33 \pm 1, 40$ degrees for a water droplet, and was used in the development of a mold. Patterned with SU-8, it made a good mold for PDMS replication. The PDMS replication was not able to capture droplets by dipping it in water, and was used as a mold for yet another replication. To realise this, it must be treated in some way. Two procedures were used. One in which a layer of Hydroxypolymethylcellulose(HPMC) was deposited on the surface. This gave a good, but hydrophilic replication. The other procedure was the silanization of the surface. The replication was not as good, but the replicated surface turned out hydrophobic.

The rough PDMS surface with smooth pillars was not able to trap water either. A final attempt to make this work was the deposition of the HPMC on the pillars.

The HPMC molecules did not adhere solely to the pillars, and most of the surface turned out hydrophilic.

The contact angle of the PDMS replication from the silanized, rough PDMS (replicated from sandpaper) gave a contact angle of $151, 29 \pm 5, 95$ with water, and is still within the definition of superhydrophobic surfaces.

4.1 *PDMS replicated from etched copper plate*

The PDMS replicated from the etched copper plate did not appear to have any great roughness, figure 4.1a, and seem to have some small cracks in the surface. The roughness is really negligent, compared to, for instance, the PDMS surface replicated from the sandpapers, figure 4.2. In addition, the surface was pretty transparent, unlike the sandpaper replicas that had opaque surfaces.

The PDMS surface was patterned in gold by photolithography, figure 4.1b. Next, the surface was treated with 1H,1H,2H,2H-Perfluorodecanethiol to make the gold hydrophobic. Unfortunately, the process did not work, and the the surface turned out to be hydrophilic. After being dipped in water, a big fraction of the surface was wetted.

The goal of this project was the trapping of water droplets by contact angle contrast. For this to work, a superhydrophobic area is required to surround an area that is less hydrophobic. Not being able to turn the gold areas hydrophobic, made this surface not eligible for trapping of droplets in the PDMS covered areas, which was the goal of this project.

4.2 *PDMS replicated from sandpapers*

The PDMS replicated directly from the three sandpapers was displayed different contact angles of water droplets on PDMS, see figure 4.2. The difference in contact angles is obvious, and the PDMS replicated from the finest sandpaper, figure 4.2a, show a very high contact angle indeed. Therefore, this was the mold used for further experiments. All the sandpaper replicated PDMS surfaces were opaque, compared to the transparent surface of smooth PDMS surfaces.

The SEM images of the PDMS replicated from the finest sandpaper seems to indicate a good replication and a high degree of roughness, figure 4.3. The x100 magnification shows $\sim 0.5\text{mm}$ features on smaller scale roughness. These seem to be small valleys on the surface.

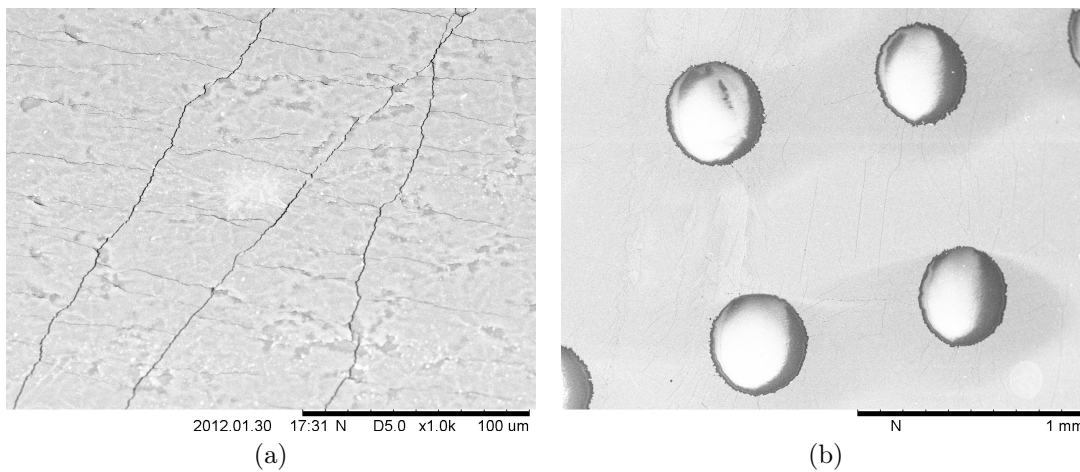


Figure 4.1: a) The PDMS made from the copper plate mold shows little roughness at x1k magnification in the SEM. The white spot in the image is a place that was zoomed in on earlier, and is an effect of poor conductance on the surface and b) The gold patterned surface after lift-off. The gold-free circles are $\sim 450\mu m$ in diameter.

It is hard to make anything from the AFM image of the surface, figure 4.4. Most of all, it shows a surface with roughness exceeding the range of height difference the AFM can handle. There also seem to be both large and small scale roughness within the $14,9 \times 14,9\mu m$ area.

From the profilometer, figure 4.5, features as large as $10\mu m$ are observed, but the features are varying a great deal in size. The difference between the x-axis and the y-axis of the graphs may be a bit misleading, as the roughness is measured in nanometers over $500\mu m$ for these graphs. The distances between the structures far exceed their height. The general tilt of the graphs could be from a tilted surface, but this could also be some larger surface structure, as the largest structures observed in the SEM are about the same size as the x-axis of the graphs.

The measured contact angles for this surface are given in table 4.1. They give a contact angle of $162,33 \pm 1,40$ degrees.

4.3 PDMS replicated from SU-8 patterned sandpaper

The PDMS replicated from SU-8 patterned sandpaper, figure 4.6, has a rough surface with smooth wells, figures 4.6b and 4.6c. The depth of these wells is hard to determine exact, but they look to be approximately $10\mu m$ in diameter. Also,



(a)

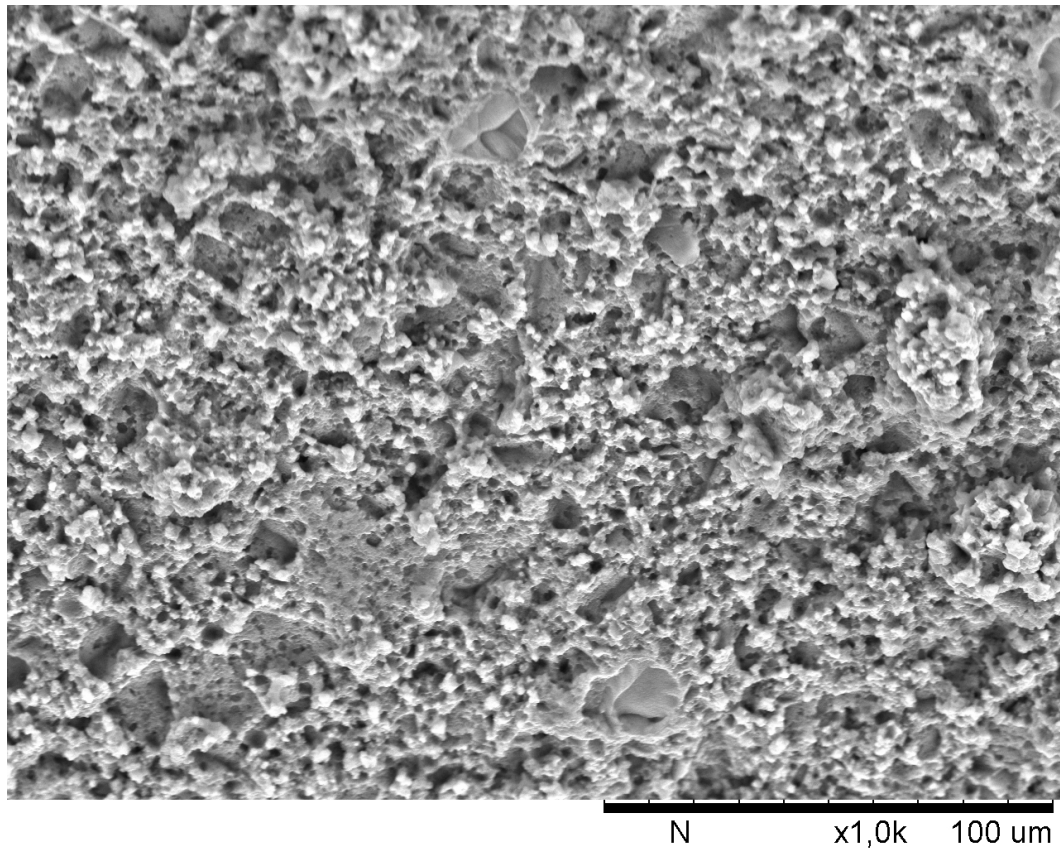


(b)

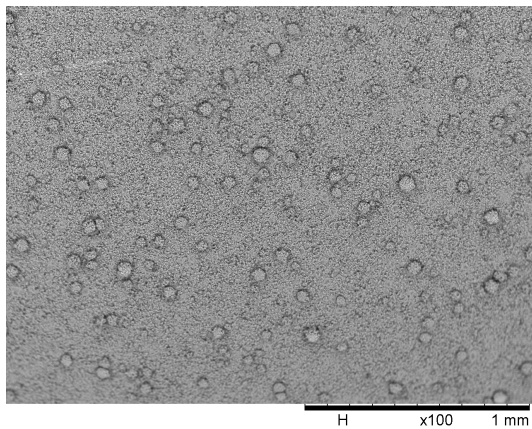


(c)

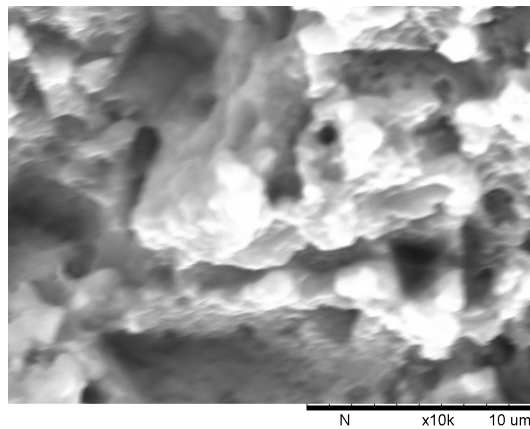
Figure 4.2: The difference in contact angle of the PDMS surface is due to the difference in roughness of the molds: a) Buehler ltd's special emery grinding paper with the grit number P1000, b) Sandpaper Nr 4/0, 30331, Schmirgelpapier Blau Deutsches Erzeugnis, Germania and c) Norton's P600 Paper Sheet T489.



(a) x1000

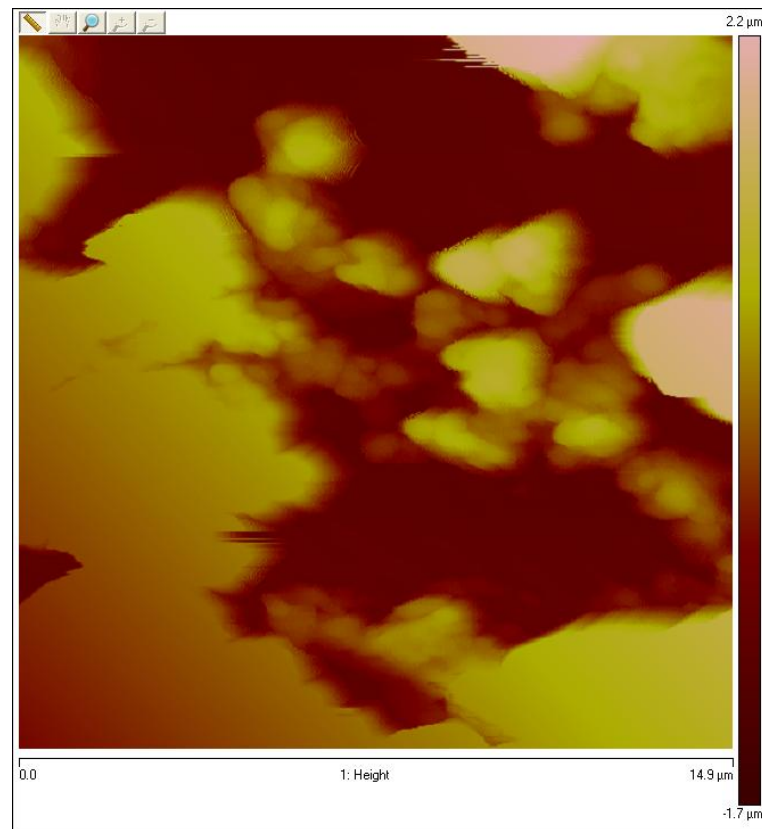


(b) x100



(c) x10,000

Figure 4.3: SEM images of a PDMS surface replicated from Buehler ltd's special emery grinding paper with the grit number P1000 at 100, 1,000 and 10,000 magnification.



(a)

Figure 4.4: AFM image of PDMS replicated from Buehler Ltd's special emery grinding paper with the grit number P1000. The image was made using tapping mode.

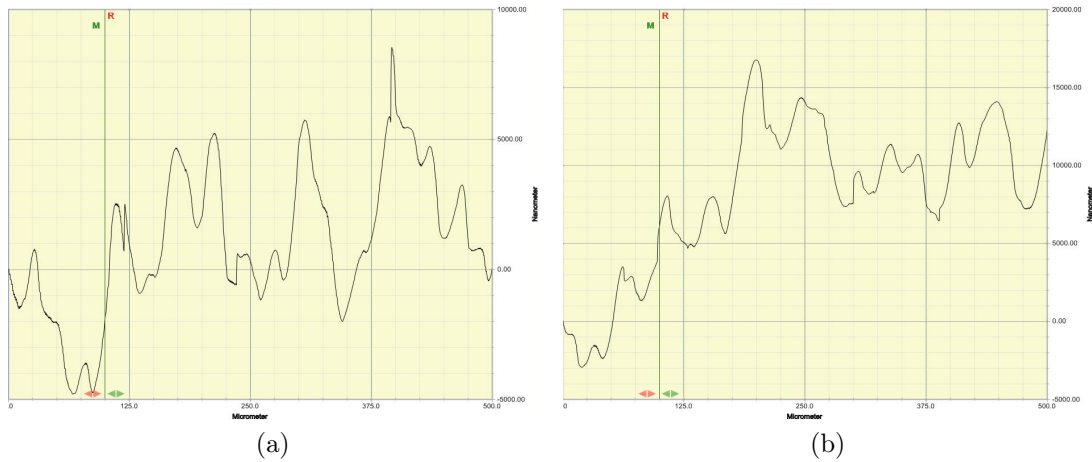


Figure 4.5: The profilometer graphs from the same replication of sandpaper into PDMS. The red and green pillars are markers, and not a part of the result.

Table 4.1: The contact angle measurements of the sandpaper-replicated PDMS and the replica from the sandpaper-replicated PDMS. The contact angle is measured on both the left and the right side of the droplet's profile.

#	Sandpaper-replicated PDMS		Replica of sandpaper-replicated PDMS	
	Left Side	Right Side	Left Side	Right Side
1	159,86	162,73	145,99	147,03
2	161,47	164,28	156,08	157,53
3	162,32	163,30	157,77	157,33
4			142,70	145,90

there are some pretty high features in the rough areas, some even higher than the depth of the wells.

The PDMS surface is depicted in figure 4.9a, and from this the well's diameter can be measured to approximately $400\mu m$ for the smallest wells. The other sandpaper mold made wells $1mm$ in diameter, these are the bigger wells.

The contact angle of the rough parts is assumed to be the same as that measured for the sandpaper-only mold, $162,33 \pm 1,40$ degrees. Dipping the surface in water, however, do not leave these parts dry and the wells with droplets, figure 4.7a. Some wells are filled with droplets, some partly filled, some not at all and some overfilled.

Trying to wet the entire surface, so that the water wetted the entire surface when

submerged, the surface was covered in ethanol before dipping it in water. This made the entire surface hydrophilic, figure 4.7.

4.4 *PDMS replicated from PDMS*

In order to achieve smooth pillars rather than smooth wells on the rough PDMS surface, efforts were made to make a new mold for PDMS replication. The requirements for such a mold was that it had smooth wells in a rough surface and could be used as a mold for PDMS replication. In addition, the PDMS replicated from such a mold must exhibit the hydrophobicity needed to test the hypothesis of the project.

The first molds to be tried out were photoresist-based molds. Both replication from rough sandpaper and from rough PDMS failed, however. This happened at the separation of the two rough surfaces. The two surfaces would simply not separate, the thick SU-8 2100 layer broke before it would release the rough PDM-S/sandpaper.

Two molds were made successfully, based on the replication of PDMS into PDMS. The PDMS surfaces with smooth wells were treated by two different chemicals, Hydroxypolymethylcellulose and Trichloro(1H,1H,2H,2H-perfluorooctyl)silane, and the treated surfaces were used as molds.

4.4.1 *Hydroxypolymethylcellulose (HPMC)*

The PDMS surface with smooth wells is treated with HPMS and used as a mold for further replication into a new PDMS surface. The PDMS replicated from HPMC-treated PDMS is easily peeled off the surface of the mold. The SEM images of this surface, figure 4.8 shows a good replication. The pillars are well defined and the rough areas look like the rough areas of the mold.

After dipping in water, the surface unfortunately turns out to be hydrophilic. Rinsing in hot water does not solve the problem.

4.4.2 *Trichloro(1H,1H,2H,2H-perfluorooctyl)silane*

As a second trial into the replication of PDMS into PDMS, the rough PDMS surface with smooth wells was treated with Trichloro(1H,1H,2H,2H-perfluorooctyl)silane. Compared to the HPMC mold, this mold would not release the PDMS as readily,

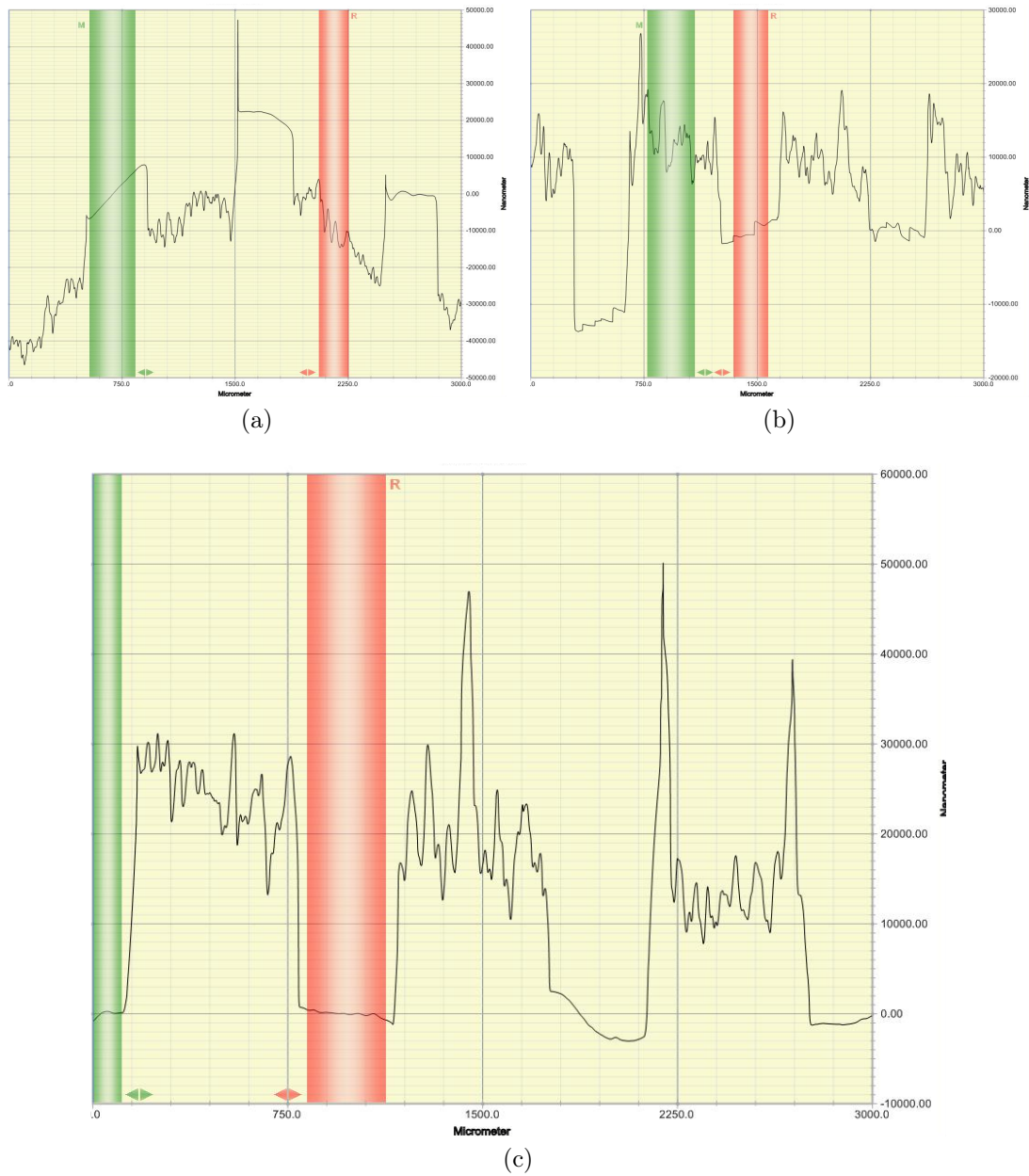
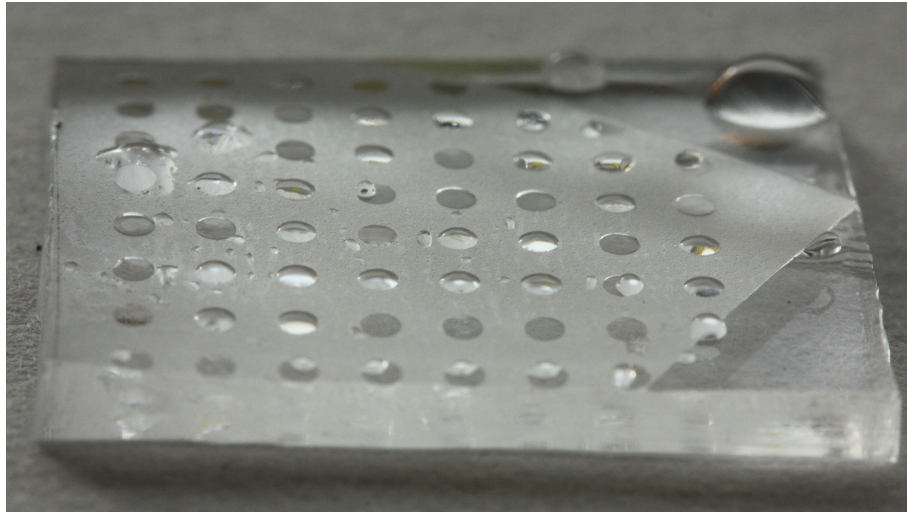
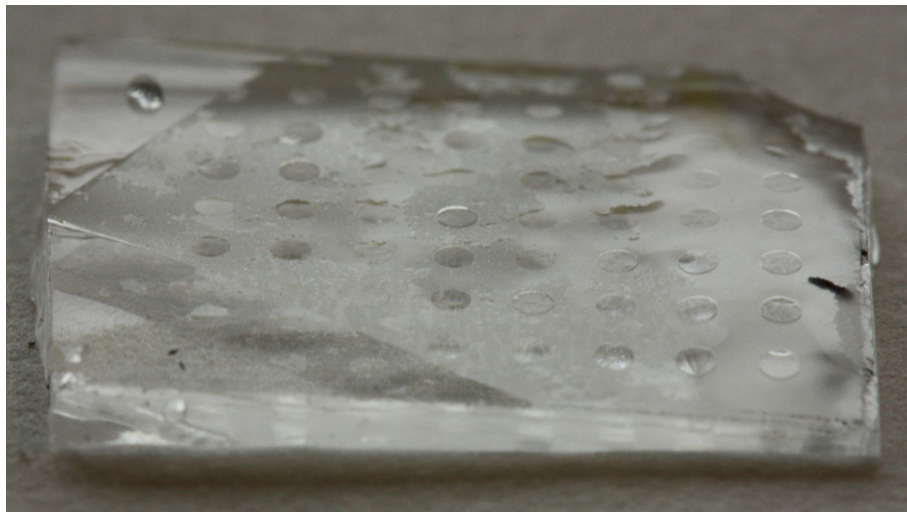


Figure 4.6: The profilometer result from a)SU-8 patterned sandpaper with $400\mu\text{m}$ pillars and b-c)the PDMS replicas of this surface. The red and green pillars are markers, and not a part of the result.

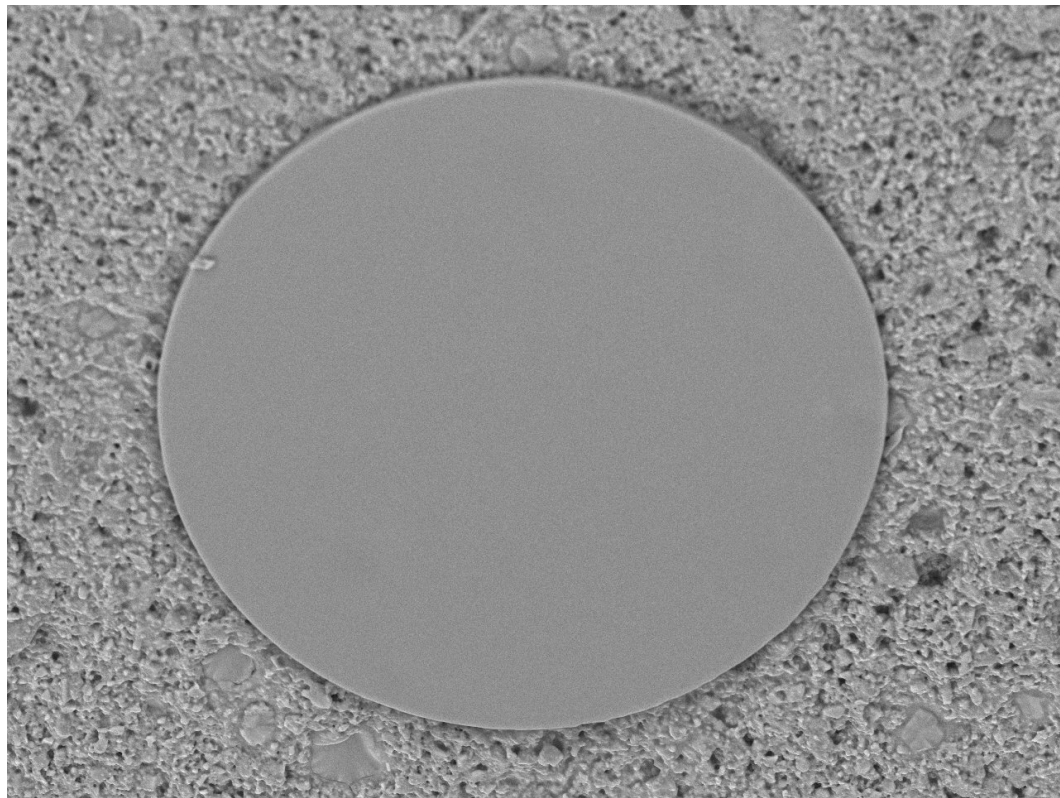


(a)



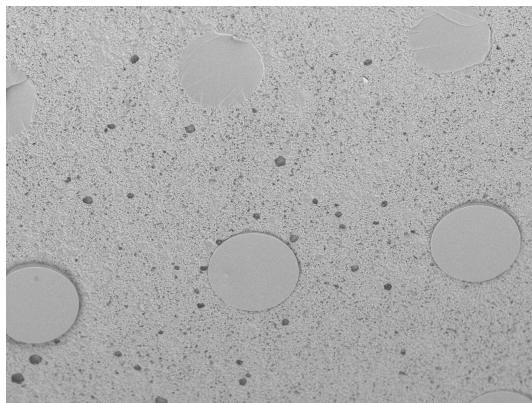
(b)

Figure 4.7: The PDMS surface produced from a SU-8 patterned sandpaper with pillars $\sim 1\text{mm}$ in diameter. The rough surface with smooth wells is depicted after a) being submerged in water and b) being firstly wetted by ethanol, then submerged in water.



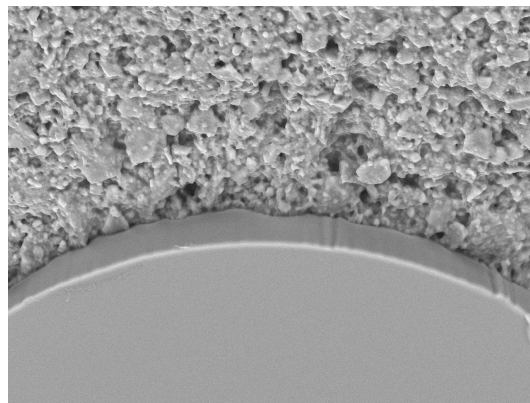
2012.04.16 13:38 NL D7,0 x400 200 um

(a) x400



2012.04.16 13:30 NL D6,3 x100 1 mm

(b) x100



2012.04.16 13:36 NL D6,3 x1,0k 100 um

(c) x1000

Figure 4.8: SEM images of the PDMS structure with flat pillars. This is replicated from HPMC treated PDMS with wells. This again, was replicated from the sandpaper-SU-8 mold with SU-8 pillars $400\mu\text{m}$ in diameter.

and the two surfaces got visibly damaged in the replication of a Trichloro(1H,1H,2H,2H-perfluorooctyl)silane treated PDMS surface that was replicated from non-patterned sandpaper. The damage was obvious when the otherwise opaque surfaces got a transparent area at separation.

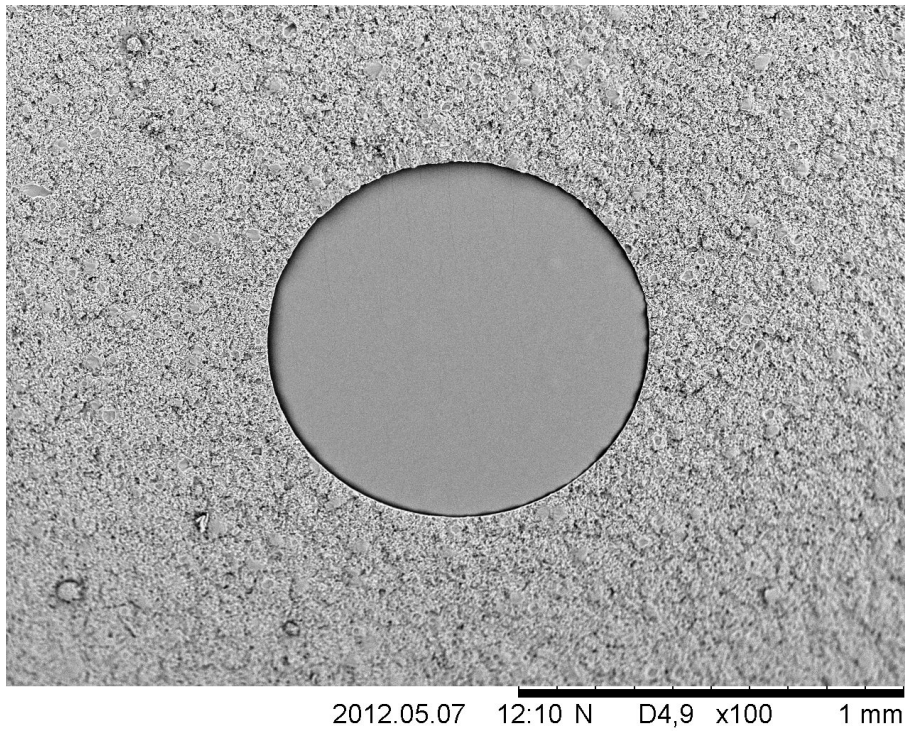
The apparently undamaged area of this surface was used for the contact angle measurements, table 4.1. While some of the rough, sandpaper-replicated PDMS was treated with Trichloro(1H,1H,2H,2H-perfluorooctyl)silane divided and replicated into a new surface, another part of the same surface was used for contact angle measurements. The difference in contact angle was noticeable, and while the sandpaper replicated PDMS surface had a measured contact angle of $162, 33 \pm 1, 40$ degrees, the surface replicated from this by the use of Trichloro(1H,1H,2H,2H-perfluorooctyl)silane, had a contact angle of $151, 29 \pm 5, 95$. The main value lies within the definition of a superhydrophobic surface, but the deviation is quite large despite more measurements than made for the sandpaper replicated PDMS surface.

The replication of the rough PDMS surface with smooth wells was replicated into a rough PDMS surface with smooth pillars, figure 4.9. The replication seemed ok, and overall, the roughness seemed to have been replicated pretty well, figure 4.10. Some features on both surfaces are less rough than the rest, and could also be a sign of PDMS replication gone wrong. The damage to the large pillars, however, is more obvious, the pillars seemed to be defected at the edges, figure 4.9b.

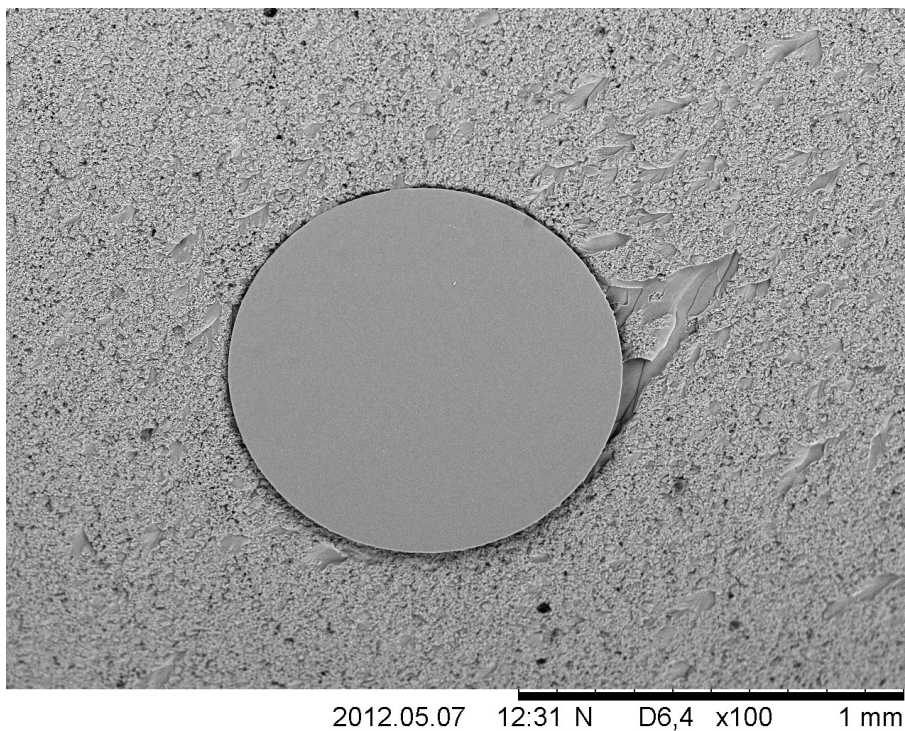
When dipped in water, the surface did not gather droplets on the smooth pillars, but the surface was hydrophobic, and did not gather droplets anywhere else either.

Hydroxypolymethylcellulose (HPMC) treatment of the pillars of The PDMS replicated by the use of Trichloro(1H,1H,2H,2H-perfluorooctyl)silane

To reduce the contact angle on the pillars and make the formation of droplets in these areas easier, the pillars were treated with HPMC deposited by a pipette. When the treated surface later was dipped in water, it was obvious that this surface was hydrophilic outside of the pillars. Actually, most of the surface seems to be hydrophilic.



(a)



(b)

Figure 4.9: SEM images of the a) smooth well of the PDMS replicated from SU-8 patterned sandpaper and b) the smooth pillar of the PDMS replicated from the silanized PDMS replicated from SU-8 patterned sandpaper. The well/pillar is approximately 1mm in diameter.

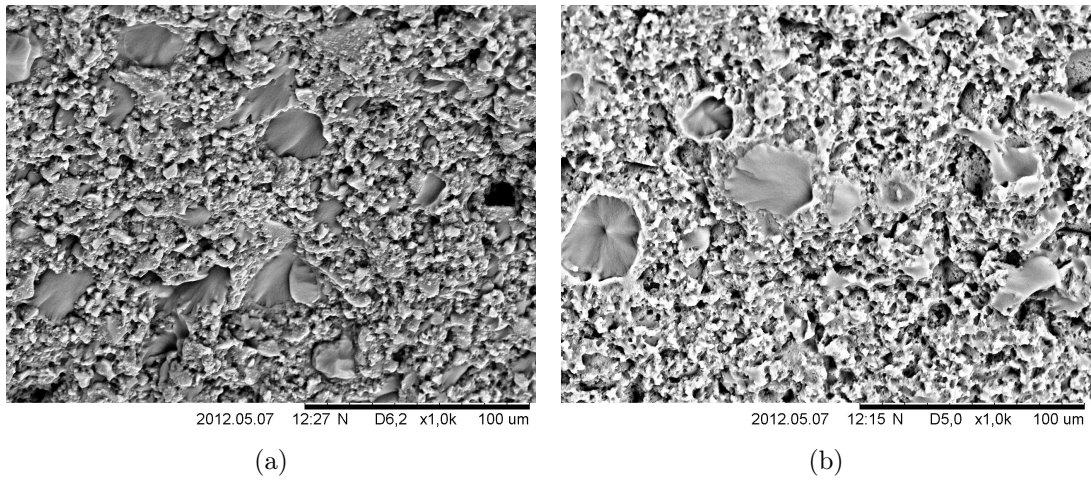


Figure 4.10: These SEM images illustrate the roughness of the a) PDMS replicated from SU-8 patterned sandpaper and b) the PDMS replication of the silanized PDMS.

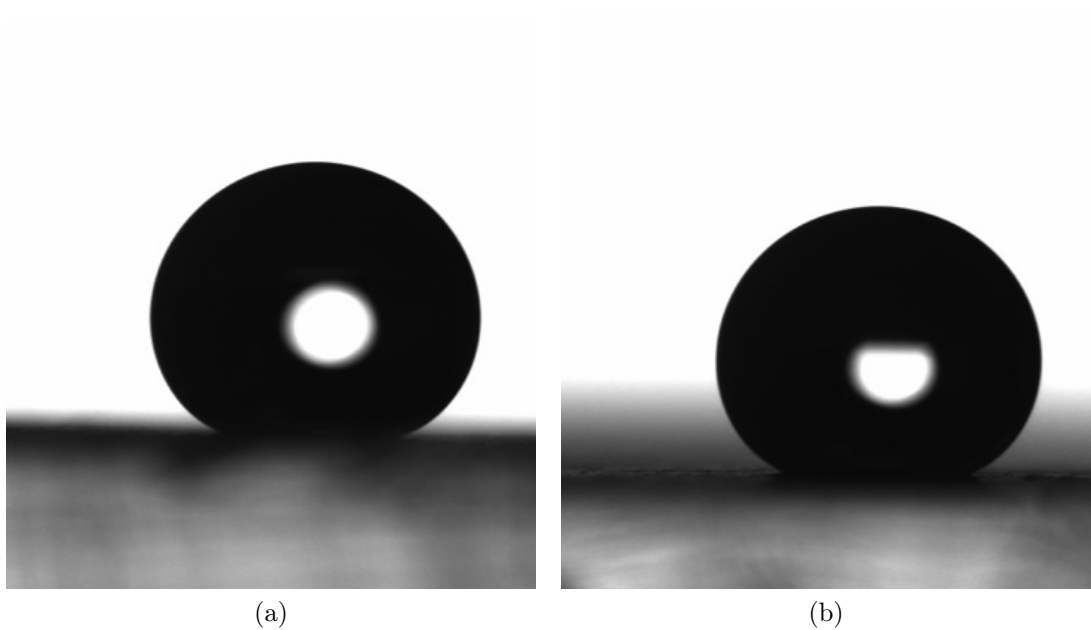


Figure 4.11: The images taken with CAM200 for the curve fitting and contact angle calculations of water droplets on a) a PDMS surface replicated from sandpaper and b) a PDMS surface replicated from a silanized PDMS surface replicated from sandpaper.

CHAPTER 5

Discussion

Contents

5.1	Etched copper as PDMS mold	59
5.2	Sandpapers as PDMS molds	60
5.3	SU-8 patterned sandpaper as PDMS mold	62
5.4	PDMS replicated from PDMS	63
5.4.1	Hydroxypolymethylcellulose (HPMC)	63
5.4.2	Trichloro(1H,1H,2H,2H-perfluorooctyl)silane	64

5.1 Etched copper as PDMS mold

The copper plates did not turn out to be all that rough, and neither did the PDMS replicated from them, see figure 4.1a. In order to examine whether flat PDMS areas surrounded by superhydrophobic material would be able to trap droplets, the replicated PDMS was further processed. Thus, the PDMS was patterned with photoresist, deposited with gold (parts of which was removed in a lift-off process) and treated with perfluorodecanethiol.

The photolithography was quite a challenge, finding a resist with a good adhesion to the surface. Since the gold pattern should be surrounding small, less hydrophobic PDMS, the photoresist was required to be patterned in small dots. Dealing with poor adhesion between the photoresist and the PDMS, this was not straightforward. The ma-n 440 negative photoresist turned out to be pretty good for this purpose, however.

The challenges did not end here, however. The perfluorodecanethiol treatment of the gold surface did not work; the surface did not become hydrophobic at all. Even when the perfluorodecanethiol treatment was done directly after lift-off, or at the

same time, the surface was still hydrophilic. Reasons for this could be that the lift-off process was done with acetone and the ethanol-based perfluorodecanethiol solution, that both tends to swell PDMS to some degree[77]. Another explanation is that the shorter, not cross-linked molecules of the PDMS migrated through/over the gold layer. Maybe the presence of the solvents somehow drew them to the surface as well.

Accordingly, this surface was not able to proof if the superhydrophobic-hydrophobic patterned surface could work to trap cells. In addition, the copper etching by this solution was too unpredictable. An adjustment of the etchant pr surface area ratio to that used in a previous project[1], was enough to alter the effect of the etchant significantly. It would demand a lot of work, if it is at all even possible, to get the copper rough enough.

5.2 Sandpapers as PDMS molds

The sandpapers used in this project was replicated into PDMS surfaces with notably different contact angles, figure 4.2. Figure 4.2a shows the PDMS with the highest contact angle, that was made from the finest of the sandpapers. For this surface, it was actually a bit of a challenge to deposit the droplets on the surface, they kept rolling off. This would not be happening for a completely plane surface, and suggest that either the mold was bulging, the PDMS cured on a surface not entirely horizontal or that the pre-PDMS was unevenly distributed over the surface before curing. The last seem to be unlikely, as even a pretty viscous liquid such as the pre-PDMS should even out before the curing stops the process.

The replication of a PDMS surface from the sandpapers was pretty straightforward, with only small difficulties in the separation of the PDMS from the sandpapers. The replicated surfaces were opaque, distinguishing them from the transparent surfaces of the smooth PDMS. This is a result of light refraction and reflection on the rough surface.

The PDMS replication of the finest sandpaper seems to be pretty good for one replication, figure 4.3, with no signs that air bubbles may have been trapped between the sandpaper and the (pre-)PDMS during replication.

It is difficult to determine the roughness of the sample by SEM, lacking a measure on the varying height over the surface. It does however indicate the roughness of the samples. In figure 4.3b, larger scale roughness is observed, with features $\sim 1\mu m$ in extent. These may be from larger features of the sandpaper: From larger emery particles or from the uneven deposition of resin used to glue the emery to the paper. For both cases, the result is a small wally on the surface. If some areas

of the sandpaper contain less emery than the rest, the result would be seen on the PDMS surface in the form of small hills on the surface. The image seem to indicate the latter.

The use of AFM was not all that helpful, see figure 4.4. Some of the difficulties may be due to the "stickiness" of the PDMS and some by the sample hitting other parts of the cantilever than the sharp tip, so that the tip cannot follow the features of the surface. With another tip, with a higher height-width ratio(that is, a longer, sharper tip), better results might have been obtained.

The height of the AFM tips used in these experiments is $15 - 20\mu m$, and the profilometer result in figure 4.6c(considered because the flat areas seem to be more level, and the image thereby more representable of the surface. It is assumed that the roughness is the same for PDMS from SU-8 patterned sandpaper as from the sandpaper alone) shows rough features up to what looks to be $\sim 30\mu m$. Considering this, it is no wonder that the AFM images of the sample are not very nice.

The profilometer manages micron scale roughness, figure 4.5, but is unfortunately only an option for measuring the height differences over a line in the sample, and for bigger structures than the AFM. Because of the tilt of the sample surface, it was difficult to determine how big features were, only how big they where combined to their neighbours, like in figure 4.5b. Comparing all the profilometer images from different samples(figures 4.5 and 4.6), the roughness seem to be varying. This could indicate a difference between mold and replica not observed by the SEM, differences over a single sandpaper surface or a result of the tilt of the samples. It could also be that the roughness of the sandpaper diminishes by each replication, and by different processing steps.

The measured contact angles for this surface varies a little. This could be because of differences in roughness over the surface, either in the sandpaper mold, replicated onto the PDMS surface or as a result of partial replication or replication errors in certain areas. Another explanation is the manual setting of the baseline on a tilted surface(the PDMS was not equally thick over the entire piece). From figure 4.11 you can see that the surface does not appear as a thin line, rather a broad, dark ribbon. This made the setting of the baseline difficult. The same tilt made depositing the droplets hard, they just kept rolling off.

Arguments can be made that the surface may well be even more hydrophobic than the measurements indicate, as they were made on areas where the droplet stuck, and might not representable of the entire surface.

Considering the variations of the measurements, the PDMS surface replicated from sandpaper give a measured contact angle of $162, 33 \pm 1, 40$ degrees. This is well within the definition of a superhydrophobic surface. It would be really interesting

to measure the roughness of the rough surfaces, but this is not possible with the equipment available for this project. Compared to the larger scale roughness of the lotus leaf, figure 1.3b, the biggest features on the rough PDMS is a smaller by a degree of 5 in extent, and look to be even smaller in height compared to the lotus leaf. Given the high contact angle of the rough PDMS, the use of sandpaper as a mold may be favorable to making a mold from a lotus leaf [78]. The use of sandpaper do not have the same limitation of surface area and is cheaper and more easily obtained than a Ni mold. The contact angle of the rough PDMS is about 1 degree lower than that replicated from a the Ni mold.

An interesting question for the further use of sandpaper as a mold to achieve superhydrophobic PDMS is how the sandpaper withstands the replications, and how many replications that can be made from a single mold. If the sandpaper turned out to be short lived, the making of a metal mold from the replicated PDMS is a possibility.

5.3 *SU-8 patterned sandpaper as PDMS mold*

The PDMS replicated from the SU-8 patterned sandpaper did not seem to be able to trap water in the smooth wells properly after being dipped in water, figure 4.7a. Some water was been trapped in the wells, and some on the rough surface. The problem seemed to be that air bubbles were trapped in the wells during immersion, and the water did not wet the surface even when submerged. This would be necessary for the wells to be filled with droplets.

However, some of the wells did (partly)fill up with water, which might suggest that the idea is realizable in some way. Maybe if the flat areas are at a level or higher than the roughness instead of below, this could work. The wetted rough areas may well be a result of sandpaper compromised in the fabrication process.

In order to wet the areas, the surface was firstly wetted with ethanol before it was immersed in the water. The ethanol was able to wet the entire surface, and upon immersion, the ethanol was replaced with water. The water also remained on the entire surface when it was removed from the water. This suggest that the Cassie-Baxter model might be the model that describes the roughnesses effect on the contact angle best for this particular surface. If the surface had been explained solely by the Wenzel model, the total wetting of the surface should to have mattered.

Also, the contact hysteresis seem to be very large for the wetted, rough surface, enough for it to display hydrophilic properties without being chemically altered at the surface. The big "droplet" on the surface just would not roll off.

In order to avoid the problem with air bubbles trapped in the wells, the making of a new mold, with surface topography like the one replicated from the SU-8 patterned sandpaper. The first idea was that a mold could be made from replication of the sandpaper or from sandpaper replicated PDMS into a photoresist mold. SU-8 was used for this purpose, SU-8 5 to cover the rough structure (like in the making of the sandpaper mold) and patterned to have small holes. This was in turn put on top of PEBing SU-8 2100. This process should create a rough photoresist structure of SU-8 5 with SU-8 2100 bottoms in the wells. Unfortunately, the sandpaper/PDMS and the photoresist could not be separated. For smooth PDMS, the replication by SU-8 is possible, so it can be assumed that it is the increased surface area due to the roughness that prohibits this.

5.4 PDMS replicated from PDMS

When the replication of the rough sandpaper/PDMS by photolithography did not work, the using of the replica as a mold was examined. Since PDMS most of all enjoys the company of PDMS, the proposed PDMS mold must be chemically altered in some way, to make the interface between the mold and the replica less favorable energetically, and thereby separable. Two different coating materials and methods were examined, the use of self assembly of HPMC and silanization by Trichloro(1H,1H,2H,2H-perfluorooctyl)silane.

5.4.1 Hydroxypolymethylcellulose (HPMC)

The use of HPMC on the PDMS mold turned out to give a really good replica. Unfortunately, the surface properties of the replicated surface was not the same as for a PDMS-only surface. The replicated surface turned out to be hydrophilic. This was unexpected, as the replicated PDMS made by *Gitlin et al.* [76] had a hydrophobic surface. The phenomenon might be explained by the varying molecule weight of HPMC, and it may be that the HPMC used in this project was of a higher molecule weight than that used by *Gitlin et al.* For bigger molecules, the HPMC might be molded into the PDMS so that hydrophilic tails protrude from the replicated surface. It does, however seem a bit strange, as the part protruding from the surface is the same that was in contact with the PDMS mold, and therefore is expected to be hydrophobic. The phenomenon seem more likely if the HPMC formed a double layer of sorts, so that the hydrophilic layer on the replica is from the molecules with hydrophobic part directed upwards and with hydrophilic tail facing the layer directly on the PDMS surface.

For this project, the rough areas need to be superhydrophobic, and this method of replication was abandoned without the access to HPMC of lower molecular weight.

5.4.2 *Trichloro(1H,1H,2H,2H-perfluorooctyl)silane*

The PDMS replicated from the Trichloro(1H,1H,2H,2H-perfluorooctyl)silane treated PDMS was fairly successful in that it made a pretty decent, hydrophobic PDMS replica. Although the replica seemed to be good at inspection after separation, SEM imaging revealed some considerable flaws in the replication. Especially around the pillars, the replication was less than perfect. This could have been due to some shadowing effects of the silanization process, foreign material on the surface that disturbed the silanization or that the silanization process was too short or that too little solution was used to cover the entire surface properly. The surface treatment was not sufficient or suitable to create a PDMS mold for a rough surface. The process may well work for less rough surfaces.

Together with the bigger flaws around the pillars, small flaws were observed on the rough parts of the surface. As the mold also showed similar flaws, these might be the result of too big adhesion, and that high aspect ratio structures were torn at separation. This is possible if the energy required to tear of a relatively small cross-section of PDMS is smaller than the energy required to separate two large, adhering interfaces. This is a result of a mold with a too high affinity for PDMS (in certain areas, at least). Improvement of the silanization process could be an answer to this. Also, the use of another fabrication method for molds might be necessary.

The contact angles of the replicated structures were noticeably smaller than those of the surface from which it was replicated, table 4.1. This could be explained either by the shape of the roughness, section 2.2.3, or by incomplete/faulty replication. This last includes: That the pre-polymer PDMS do not follow the surface it is supposed to replicate or that the two pieces of PDMS stick too well to each other in certain areas, and that pieces of PDMS were ripped off and stayed in/on the other PDMS surface.

The actual test of the surface was in the immersion of water. The surface was not able to trap water in the smooth areas. Not at all. Although the contact angle is less than for the sandpaper-replicated PDMS, it is still hydrophobic. That is assuming that the replica from a silanized sandpaper-replicated PDMS (without any wells) replicate similarly to the replication of the PDMS replicated from the silanized PDMS replicated from SU-8 patterned sandpaper.

For other, less rough surfaces, the replication by this means may be better, as the ratio of the actual surface area and the surface area calculated from the shape of the piece of material will be lower, and more easily separated. In addition,

the absence of high aspect ratio structures will decrease the possibility that such structures are ripped off.

As to the idea of water capturing to certain areas of PDMS only by manipulating the surface roughness, the smooth wells approach seem to be better. Maybe a smooth area on the same level as the roughness would do even better, but there is a distinctive chance that the idea is not realizable. The PDMS would still be hydrophobic in the smooth areas, and by definition repel water. To be certain a device would work, there would have to be both a hydrophilic water capturing area and a superhydrophobic area repelling water. A last attempt was made at creating this.

Hydroxypolymethylcellulose (HPMC) treatment of the pillars of The PDMS replicated by the use of Trichloro(1H,1H,2H,2H-perfluorooctyl)silane

The treatment of HPMC of the pillars on the PDMS surface turned out to make most of the surface hydrophilic, and not only the pillars. The intension was that the surface would be superhydrophobic in the rough areas and hydrophilic in the smooth areas on top of the pillars. However this did not work.

The HPMC has a part that favors the hydrophobic PDMS. However, it favors the rough, superhydrophobic PDMS even more, and the HPMC molecules must have attached to these parts as well during the treatment and/or during the water rinsing. This is an effect of the design of the surface and cannot be avoided without major adjustments of the process. Such adjustments could be some kind of protection layer/mask over the superhydrophobic surface, treatment to make the smooth parts hydrophilic and removal of the protection layer/mask.

CHAPTER 6

Conclusion

In this project roughness only has been used to create areas of different contact angles on a PDMS surface. The aim of this was the fabrication of a surface able of water capturing to certain areas, and ultimately the capturing of a cellular suspension to the same areas. Roughness of hydrophobic surfaces will have the effect of increasing the observed contact angle and making the surface more hydrophobic than it would have been had it been perfectly smooth.

PDMS is such a hydrophobic material, and by the replication from different molds, PDMS surfaces were created with rough areas surrounding smaller, smooth areas. The smooth areas ($400\mu\text{m}$ and 1mm in diameter) were produced to be both elevated over the roughness and at a lower level than the roughness. Regardless, the surfaces was not able to achieve the water capturing ability that was the goal of the project. Although, the rough surface with smooth wells was able to capture some water. However, the wells were not totally filled, and some were not filled at all. If more work is done on this idea, the development of smooth areas at the level of the roughness, or below, seem to be more promising than smooth pillars.

Between the etched copper plates and sandpapers, the sandpapers turned out to be the simplest, cheapest and best molds for producing a high degree of roughness on a PDMS surface. Of the tested sandpapers, the Buehler ltd's special emery grinding paper with the grit number P1000 gave the highest contact angle for a water droplet on the sandpaper-replicated PDMS. While the contact angle of a smooth PDMS surface is $101.8 \pm 3.4^\circ$, the rough, sandpaper replicated PDMS had a contact angle of $162, 33 \pm 1, 40^\circ$ for water.

Accordingly, it is possible to create a superhydrophobic PDMS surface from a mold of sandpaper. The simplicity and cost of the sandpaper mold is a great advantage for this route of production, which is both easier and cheaper than other means of production.

As mentioned earlier, the project failed to produce a good enough water capturing PDMS surface with patterned roughness. Different approaches were examined,

but even with a contrast between the rough and smooth areas of $\sim 61^\circ$ for the rough structures with smooth wells and $\sim 50^\circ$ for the rough structure with smooth pillars, the water capturing did not work. A better replication method for the rough surface with smooth pillars might improve the results. This produced a contact angle with water 10° less than the structure it was replicated from. Although this might be an effect of a skewness(explained in theory) of the sandpaper, it might as well be an effect of partial replication. SEM images seem to suggest this.

The major achievement of the project is the production of a rough PDMS surface from sandpaper. A simple, cheap and good mold to create superhydrophobic PDMS. Developing the idea could include emery particles in paints, on windows(covered with a thin hydrophobic layer) or by other means use the roughness of the particles in applications where hydrophobicity/hydrophilicity might be favorable.

Bibliography

- [1] Brita Melberg. Nanostructured PDMS surfaces with patterned wettability. 2011.
- [2] Thor Christian Hobæk. Nanostructured PDMS surfaces with patterned wettability. Master's thesis, NTNU, 2011.
- [3] Didier Falconnet, Gabor Csucs, H Michelle Grandin, and Marcus Textor. Surface engineering approaches to micropattern surfaces for cell-based assays. *Biomaterials*, 27(16):3044–63, June 2006.
- [4] Manuel Théry. Micropatterning as a tool to decipher cell morphogenesis and functions. *Journal of cell science*, 123(Pt 24):4201–4213, 2010.
- [5] Sara M Oliveira, Wenlong Song, Natalia M Alves, and Joao F Mano. Chemical modification of bioinspired superhydrophobic polystyrene surfaces to control cell attachment/proliferation. *Soft Matter*, 7(19):8932–8941, 2011.
- [6] Villa Painting - Spray Application Specialists.
- [7] Y Y Liu, R H Wang, H F Lu, L Li, Y Y Kong, K H Qi, and J H Xin. Artificial lotus leaf structures from assembling carbon nanotubes and their applications in hydrophobic textiles. *Journal of Materials Chemistry*, 17(11):1071–1078, 2007.
- [8] HyperPhysics, Surface Tension.
- [9] Ramé-Hart Information on Contact Angle. [\url{http://www.ramehart.com/contactangle.htm}](http://www.ramehart.com/contactangle.htm), November 2011.
- [10] D Quere and David Quéré. Non-sticking drops. *Reports on Progress in Physics*, 68(11):2495–2532, November 2005.
- [11] Bharat Bhushan. *Introduction to Tribology*. Wiley, 2002.
- [12] JACC report No 26 -Linear Polydimethylsiloxanes. Technical report, European Centre for Ecotoxicology and Toxicology of chemicals, September 1994.

- [13] D J Campbell, K J Beckman, C E Calderon, P W Doolan, R M Ottosen, A B Ellis, and G C Lisensky. Replication and compression of bulk and surface structures with polydimethylsiloxane elastomer. *Journal of Chemical Education*, 76(4):537–541, 1999.
- [14] Sigma-Aldrich, 1H,1H,2H,2H-Perfluorodecanethiol.
- [15] A del Campo and C Greiner. SU-8: a photoresist for high-aspect-ratio and 3D submicron lithography. *JOURNAL OF MICROMECHANICS AND MICROENGINEERING*, 17(6):R81–R95, June 2007.
- [16] Purdue University, Scanning Electron Microscope. [\url{http://www.purdue.edu/rem/rs/sem.htm}](http://www.purdue.edu/rem/rs/sem.htm), 2011.
- [17] Interaction of electron beams with matter, Surface & Plasma Technology Research Group of the Institut für Allgemeine Physik. [\url{http://eaps4.iap.tuwien.ac.at/~werner/qes_tut_interact.htm}](http://eaps4.iap.tuwien.ac.at/~werner/qes_tut_interact.htm), 2011.
- [18] Hitachi Tabletop Microscope TM3000, 2010.
- [19] NanoScience Instruments: AFM. [\url{http://www.nanoscience.com/education/afm.html}](http://www.nanoscience.com/education/afm.html), 2011.
- [20] Bharat Bhushan, editor. *Springer Handbook of Nanotechnology*. Springer Berlin Heidelberg, 2007.
- [21] Metrology of Thin Films, Wafer Bumping.
- [22] Manuel Théry and Matthieu Piel. Adhesive micropatterns for cells: a microcontact printing protocol. *Cold Spring Harbor protocols*, 2009(7):pdb.prot5255, 2009.
- [23] Bruker AFM probes, MPP-11100-10.
- [24] KSV Instruments Ltd. *CAM200*. KSV Instruments Ltd, Finland.
- [25] Moo-Yeal Lee, R Anand Kumar, Sumitra M Sukumaran, Michael G Hogg, Douglas S Clark, and Jonathan S Dordick. Three-dimensional cellular microarray for high-throughput toxicology assays. *Proceedings of the National Academy of Sciences of the United States of America*, 105(1):59–63, 2008.
- [26] Shannon B Falconer and Eric D Brown. New screens and targets in antibacterial drug discovery. *Current Opinion in Microbiology*, 12(5):497–504, October 2009.

- [27] Saravanan Rajan, Haig Djambazian, Huan Chu Pham Dang, Rob Sladek, and Thomas J Hudson. The living microarray: a high-throughput platform for measuring transcription dynamics in single cells. *BMC genomics*, 12(1):115, 2011.
- [28] Christopher M Dobson. Chemical space and biology. *Nature*, 432(7019):824–828, December 2004.
- [29] H Mario H M Geysen, Frank F Schoenen, David D Wagner, and Richard R Wagner. Combinatorial compound libraries for drug discovery: an ongoing challenge. *Nature reviews. Drug discovery*, 2(3):222–230, 2003.
- [30] Derek S Tan. Diversity-oriented synthesis: exploring the intersections between chemistry and biology. *Nat Chem Biol*, 1(2):74–84, July 2005.
- [31] Greiner Bio-One Microplate Dimensions Guide. [\url{http://www.greinerbioone.com/en/row/articles/catalogue/article-groups/2_11/}](http://www.greinerbioone.com/en/row/articles/catalogue/article-groups/2_11/), 2012.
- [32] Allison D Ebert and Clive N Svendsen. Human stem cells and drug screening: opportunities and challenges. *Nat Rev Drug Discov*, 9(5):367–372, May 2010.
- [33] M L Yarmush and K R King. Living-Cell Microarrays. *Annu. Rev. Biomed. Eng.*, 11:235–257, 2009.
- [34] Michael Sixt and Tim Lämmermann. In Vitro Analysis of Chemotactic Leukocyte Migration in 3D Environments. In Claire M Wells and Maddy Parsons, editors, *CELL MIGRATION -Methods in Molecular Biology*, volume 769 of *Methods in Molecular Biology*, pages 149–165. Humana Press, 2011.
- [35] Jinghua Han, Fei Zhang, Man Yu, Peiqi Zhao, Wei Ji, Haichang Zhang, Bing Wu, Yuqing Wang, and Ruifang Niu. RNA interference-mediated silencing of NANOG reduces cell proliferation and induces G0/G1 cell cycle arrest in breast cancer cells. *Cancer Letters*, 321(1):80–88, August 2012.
- [36] Muthu K Shanmugam, An H Nguyen, Alan P Kumar, Benny K H Tan, and Gautam Sethi. Targeted inhibition of tumor proliferation, survival, and metastasis by pentacyclic triterpenoids: Potential role in prevention and therapy of cancer. *Cancer Letters*, 320(2):158–170, July 2012.
- [37] David A Brafman, Shu Chien, and Karl Willert. Arrayed cellular microenvironments for identifying culture and differentiation conditions for stem, primary and rare cell populations. *NATURE PROTOCOLS*, 7(4):703–717, April 2012.

- [38] Chiara Stringari, Robert Sierra, Peter J Donovan, and Enrico Gratton. Label-free separation of human embryonic stem cells and their differentiating progenies by phasor fluorescence lifetime microscopy. *Journal of Biomedical Optics*, 17(4):46012, 2012.
- [39] Tadato Ban, Masaru Hoshino, Satoshi Takahashi, Daizo Hamada, Kazuhiro Hasegawa, Hironobu Naiki, and Yuji Goto. Direct observation of Abeta amyloid fibril growth and inhibition. *Journal of molecular biology*, 344(3):757–767, November 2004.
- [40] VistaGen.
- [41] Anna Tourovskaia, Thomas Barber, Bronwyn T Wickes, Danny Hirdes, Boris Grin, David G Castner, Kevin E Healy, and Albert Folch. Micropatterns of Chemisorbed Cell Adhesion-Repellent Films Using Oxygen Plasma Etching and Elastomeric Masks. *Langmuir*, 19(11):4754–4764, 2003.
- [42] N Blondiaux, E Scolan, A M Popa, J Gavillet, and R Pugin. Fabrication of superhydrophobic surfaces with controlled topography and chemistry. *APPLIED SURFACE SCIENCE*, 256(3, 1):S46–S53, November 2009.
- [43] Barbara Cortese, Stefania D’Amone, Michele Manca, Ilenia Viola, Roberto Cingolani, and Giuseppe Gigli. Superhydrophobicity Due to the Hierarchical Scale Roughness of PDMS Surfaces. *Langmuir*, 24(6):2712–2718, 2008.
- [44] Z P Fan, W L Liu, Z J Wei, J S Yao, X L Sun, M Li, and X Q Wang. Fabrication of two biomimetic superhydrophobic polymeric surfaces. *Applied Surface Science*, 257(9):4296–4301, 2011.
- [45] K Ellinas, A Tserepi, and E Gogolides. From Superamphiphobic to Amphiphilic Polymeric Surfaces with Ordered Hierarchical Roughness Fabricated with Colloidal Lithography and Plasma Nanotexturing. *Langmuir*, 27(7):3960–3969, 2011.
- [46] Shuaixia Tan, Qiongdan Xie, Xiaoying Lu, Ning Zhao, Xiaoli Zhang, and Jian Xu. One step preparation of superhydrophobic polymeric surface with polystyrene under ambient atmosphere. *Journal of Colloid and Interface Science*, 322(1):1–5, 2008.
- [47] W L Song, A C Lima, and J F Mano. Bioinspired methodology to fabricate hydrogel spheres for multi-applications using superhydrophobic substrates. *Soft Matter*, 6(23):5868–5871, 2010.

- [48] N M Oliveira, A I Neto, W L Song, and J F Mano. Two-Dimensional Open Microfluidic Devices by Tuning the Wettability on Patterned Superhydrophobic Polymeric Surface. *Applied Physics Express*, 3(8), 2010.
- [49] Preben C Mørk. *Overflate og kolloidkjemi -Grunnleggende prinsipper og teorier*. Norges teknisk-naturvitenskapelige universitet, 2004.
- [50] Richard M Pashley and Marilyn E Karaman. *Applied Colloid and Surface Chemistry*. Wiley, 2004.
- [51] H Yildirim Erbil. *Surface Chemistry of Solid and Liquid Interfaces*. Blackwell Publishing, 2006.
- [52] Bharat Bhushan, Michael Nosonovsky, and Yong Chae Jung. Towards optimization of patterned superhydrophobic surfaces. *Journal of The Royal Society Interface*, 4(15):643–648, 2007.
- [53] Krister Holmberg. Handbook of Applied Surface and Colloid Chemistry, Volumes 1-2.
- [54] Gene Whyman, Edward Bormashenko, and Tamir Stein. The rigorous derivation of Young, Cassie, Baxter and Wenzel equations and the analysis of the contact angle hysteresis phenomenon. *Chemical Physics Letters*, 450(4-6):355–359, January 2008.
- [55] Dorota I Rozkiewicz, Yvonne Kraan, Marc W T Werten, Frits a de Wolf, Vinod Subramaniam, Bart Jan Ravoo, and David N Reinhoudt. Covalent microcontact printing of proteins for cell patterning. *Chemistry (Weinheim an der Bergstrasse, Germany)*, 12(24):6290–6297, August 2006.
- [56] Linfen Yu, Huaiqing Huang, Xiuling Dong, Dapeng Wu, Jinhua Qin, and Bingcheng Lin. Simple, fast and high-throughput single-cell analysis on PDMS microfluidic chips. *ELECTROPHORESIS*, 29(24):5055–5060, 2008.
- [57] Robert D Lovchik, Noemi Tonna, Fabio Bianco, Michela Matteoli, and Emmanuel Delamarche. A microfluidic device for depositing and addressing two cell populations with intercellular population communication capability. *Biomedical microdevices*, 12(2):275–282, April 2010.
- [58] James Patterson Bailey and Bernard. *Solid-State Physics Introduction to the Theory*. Springer Berlin Heidelberg, 2010.
- [59] Jianting Che Zhike Wang and Cunling Ye. Application of ferric chloride both as an oxidant and complexant to enhance the dissolution of metallic copper. *Hydrometallurgy*, 105(69-74), 2010.

- [60] Yoshlro Yoshihiro Shln-lchi Habu. Studies of Copper Etching in Ferric Chloride Solutions. *Industrial and Engineerring Chemistry Process Design and Development*, 21(3):511–514, 1982.
- [61] S Habu and Y Yoshihiro. STUDIES OF COPPER ETCHING IN FERRIC-CHLORIDE SOLUTIONS. *Industrial and Engineering Chemistry Process Design and Development*, 21(3):511–514, 1982.
- [62] Miaojun Xu, Nan Lu, Dianpeng Qi, Hongbo Xu, Yandong Wang, Shoulei Shi, and Lifeng Chi. Fabrication of superhydrophobic polymer films with hierarchical silver microbowl array structures. *Journal of Colloid and Interface Science*, 360(1):300–304, August 2011.
- [63] J Christopher Love, Lara A Estroff, Jennah K Kriebel, Ralph G Nuzzo, and George M Whitesides. Self-Assembled Monolayers of Thiolates on Metals as a Form of Nanotechnology. *Chemical Reviews*, 105(4):1103–1170, March 2005.
- [64] J Liu, B Cai, J Zhu, G Ding, X Zhao, C Yang, and D Chen. Process research of high aspect ratio microstructure using SU-8 resist. *Microsystem Technologies*, 10(4):265–268, 2004.
- [65] MicroChem, Nano SU-8 manual.
- [66] MicroChem, SU-8 2000 manual.
- [67] Michael Quirk and Julian Serda. *Semiconductor Manufacturing Technology*. Publishing House of Electronics Industry, 2006.
- [68] Zhong Lin Wan Weilie Zhou, editor. *Scanning Microscopy for Nanotechnology*. Springer, 2007.
- [69] Bjørn T Stokke de Lange Davies. Lecture notes TFY 4265Biophysical Microtechniques. Department of Physics, NTNU.
- [70] D Kaczmarek. Backscattered electrons topographic mode problems in the scanning electron microscope. *Optica Applicata*, 31(3):649–658, 2001.
- [71] Bradley L Thiel. Image Formation in Low Vacuum SEM. *Microchimica Acta*, 145(1):243–247, April 2004.
- [72] John Kuo, editor. *Electron Microscopy Methods and Protocols*. SpringerLink, 2007.
- [73] Quorum Technologies. Sputter Coating Sputter Coater, Technical Brief. Technical Report Document Number TB-SPUTTER, Quorum Technologies, 2002.

- [74] Henning Klank Oliver Geschke and Pieter Telleman, editors. *Microsystem Engineering of Lab-on-a-Chip Devices*. Wiley-VCH, 2008.
- [75] *Buehler Sum-Met: The science behind Materials Preparation*, 2004.
- [76] Leonid Gitlin, Philipp Schulze, and Detlev Belder. Rapid replication of master structures by double casting with PDMS. *Lab Chip*, 9(20):3000–3002, 2009.
- [77] J N Lee, C Park, and G M Whitesides. Solvent compatibility of poly (dimethylsiloxane)-based microfluidic devices. *Anal. Chem.*, 75(23):6544–6554, 2003.
- [78] Seung-Mo Lee and Tai Hun Kwon. Effects of intrinsic hydrophobicity on wettability of polymer replicas of a superhydrophobic lotus leaf. *Journal of Micromechanics and Microengineering*, 17(4):687–692, April 2007.